# LANGMUIR

pubs.acs.org/Langmuir Article

# Force Field Parameter Development for the Thiolate/Defective Au(111) Interface

Guobing Zhou, Chang Liu, Lloyd A. Bumm, and Liangliang Huang\*



Cite This: Langmuir 2020, 36, 4098-4107



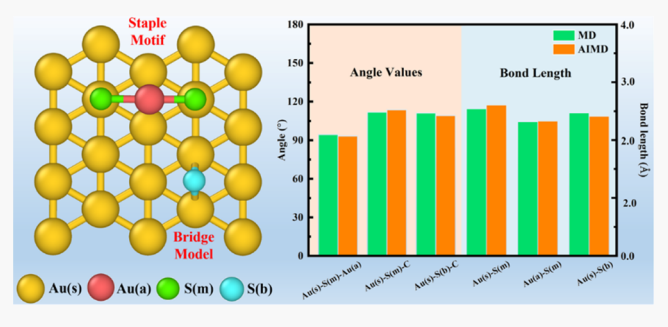
**ACCESS** 

III Metrics & More

Article Recommendations

Supporting Information

ABSTRACT: A molecular-level understanding of the interplay between self-assembled monolayers (SAMs) of thiolates and gold surface is of great importance to a wide range of applications in surface science and nanotechnology. Despite theoretical research progress of the past decade, an atomistic model, capable of describing key features of SAMs at reconstructed gold surfaces, is still missing. In this work, periodic ab initio density functional theory (DFT) calculations were utilized to develop a new atomistic force field model for alkanethiolate (AT) SAMs on a reconstructed Au(111) surface. The new force field parameters were carefully trained to reproduce the key features, including vibrational spectra



and torsion energy profiles of ethylthiolate ( $C_2S$ ) in the bridge or staple motif model on the Au(111) surface, wherein, the force constants of the bond and angle terms were trained by matching the vibrational spectra, while the torsion parameters of the dihedral angles were trained via fitting the torsion energy profiles from DFT calculations. To validate the developed force field parameters, we performed classical molecular dynamics (MD) simulations for both pristine and reconstructed Au–S interface models with a ( $2\sqrt{3} \times 3$ ) unit cell, which includes four dodecanethiolate ( $C_{10}S$ ) molecules on the Au(111) surface. The simulation results showed that the geometrical features of the investigated Au–S interface models and structural properties of the  $C_{10}S$  SAMs are in good agreement with the ab initio MD studies. The newly developed atomistic force field model provides new fundamental insights into AT SAMs on the reconstructed Au(111) surface and adds advancement to the existing interface research knowledge.

#### 1. INTRODUCTION

Self-assembly of thiolates on the gold surface has received extensive attention in nanotechnology, material science, and surface science. The for those generated self-assembled monolayers (SAMs) on gold substrates, their properties are significantly influenced by the structural and chemical properties of the gold—thiolate interface. The interfacial gold—sulfur (Au—S) interactions, comparable to the strength of gold—gold bonding, are accepted to play a critical role to stabilize the gold substrate and regulate the functionality of SAMs. Over the past decades, increasing research interest has been devoted to understanding the molecular nature of the Au—S interface to further promote their applications in nanoelectronics, biological sensing, molecular recognition, heterogeneous catalysis, and drug delivery, to just name a few.

On the other hand, since the discovery of alkylamines SAMs on Pt by Bigelow et al., <sup>12</sup> experimental techniques, such as scanning tunneling microscopy, grazing-incidence X-ray diffraction (GIXRD), X-ray standing waves, X-ray photoelectron spectroscopy, and low-energy electron diffraction (LEED), coupled with density functional theory (DFT) calculations, have been routinely utilized to detect the structural evolution of the Au–S interface. <sup>1,2,4,5,7,13–15</sup> For example, Nuzzo and coworkers proposed that the Au–S

interface is defect-free and S atoms of the thiolates are adsorbed via the three-fold hollow sites of the Au(111) surface. 16 Later, DFT calculation results revealed that the bridge sites seem to be more energetically stable for the adsorption of alkanethiolate (AT) on the pristine Au(111) surface. 17-21 With the advancement of characterization tools, nowadays, it is accepted that the pristine Au(111) surface could undergo reconstruction during thiolate adsorption, to generate vacancies and adatoms of the gold substrate and promote different binding sites for S atoms.<sup>2,5-7,15,22</sup> Of those defective models, the staple motif (S-Au<sub>ad</sub>-S) model has been recommended, where an intermediate Au adatom is bonded with two S atoms located atop the Au atoms in the first layer of the substrate.<sup>5,7</sup> Combining GIXRD experiments and DFT calculations, Scoles and coworkers also proposed a staple motif model where S atoms of thiolates are laterally bound to two Au adatoms of the bridge sites. 15 Additionally, Chaudhuri et al. 23

Received: February 24, 2020 Revised: March 19, 2020 Published: March 22, 2020





found a completely different adsorption configuration to uncover the  $(2\sqrt{3}\times 3)$  rect. phase of butylthiolate SAMs on Au(111). Their LEED experiments show that S atoms of thiolates are located at the top Au adatoms of FCC and HCP hollow sites.

Extensive theoretical efforts have been also developed to the understanding of adatoms and vacancies of gold substrates and how they affect the packing configuration and stability of SAMs. 4,15,24-26 DFT calculations of Wang and Selloni 24 showed that the packing structures of  $c(4 \times 2)$  AT SAMs are remarkably different from the previously accepted  $(\sqrt{3} \times \sqrt{3})R30^{\circ}$  configuration, if the adatom/vacancy of the gold substrate is considered. Torres et al. 25 investigated the role of Au adatoms to high-density ethylthiolate (ET) SAMs, and their DFT calculations revealed that the number of gold adatoms can significantly influence SAM stability. By comparing the binding and surface energies, they demonstrated that the SAM is most stable where two ET-Au-ET adatom moieties are on the top of surface Au atoms.<sup>25</sup> Similarly, a large number of classical molecular dynamics (MD) simulations have been also employed to understand the behavior of SAMs.<sup>27–31</sup> However, we note that with the better understanding of defective gold substrate characteristics, a reparameterization is necessary of force fields to better describe SAM/Au systems.

In this work, we performed a series of DFT and MD simulations to develop force field parameters to accurately describe AT SAMs on the reconstructed Au(111) surface. Those bonded force field parameters were trained to reproduce key features (vibrational spectra and torsion energy profiles) of the bridge and staple motif ethylthiolate (C2S) models on the pristine Au(111) surface. In specific, the force constants of bond and angle terms were trained by matching the vibrational spectra of DFT results. The torsion parameters were optimized via fitting the torsion energy profile of MD to that of DFT calculations. The retrained force field parameters are applied to study pristine and reconstructed Au-dodecanethiolate (C<sub>10</sub>S) SAMs with a  $(2\sqrt{3} \times 3)$  unit cell, and agree well with ab initio molecular dynamics (AIMD) simulation results. The paper is organized as follows: In Section 2, we describe simulation methods and calculation details. Discussion of the force field fitting and MD and DFT results are presented in Section 3. Force field validations will be provided in Section 4. Finally, Section 5 has general conclusions and remarks.

#### 2. METHODS AND SIMULATION DETAILS

2.1. Ab-Initio DFT Calculation. The DFT calculations are performed using the Vienna Ab initio Simulation Package (VASP) of the MedeA computational platform.<sup>32</sup> The ion–electron interactions were described through the projector-augmented wave method,<sup>33</sup> and the electron exchange and correlation interactions were represented by the generalized gradient approximation of the Perdew–Burke– Ernzerhof functional.<sup>34</sup> The van der Waals interactions were included through the Grimme's DFT-D3 semi-empirical method.  $^{35}$  A cutoff energy of 450 eV was adopted for the plane-wave basis set, and all calculations were carried out using Gaussian smearing with a width of 0.2 eV. The ionic relaxation was converged until the atomic force is less than 0.01 eV Å-1, and the self-consistency was subjected to the successive energy difference of 10<sup>-5</sup> eV. The slab method was applied to model the Au(111) surface with four atomic layers and a vacuum of 15 Å was added above the surface to avoid the interactions between periodic images. The Au(111) surface consists of a  $(2\sqrt{3} \times 3)$  unit cell with 12 Au atoms per layer, and the lateral simulation dimensions were  $8.70 \times 10.04 \text{ Å}^2$ . During geometry optimization, the entire gold

surface was fixed to represent the bulk structure, with the remaining parts being flexible. The obtained equilibrium configurations were used for subsequent calculations. It should be noted that for the vibrational frequency analysis, the entire gold substrate was fixed in both MD and DFT calculations. Among all calculations, the first Brillouin zone was sampled with  $6\times6\times1$  k-points.

**2.2. Force Field Potential.** The force field used in this study to calculate the potential energy has the following functional forms

$$U = \sum_{\text{bonds}} K_{\text{b}} (r - r_0)^2 + \sum_{\text{angles}} K_{\theta} (\theta - \theta_0)^2$$

$$+ \sum_{\text{dihedrals}} \sum_{n=1}^4 \frac{K_n}{2} [1 + \cos(n\phi - \gamma)] + 4\varepsilon_{ij} \left[ \left( \frac{\sigma_{ij}}{r_{ij}} \right)^{12} - \left( \frac{\sigma_{ij}}{r_{ij}} \right)^6 \right]$$

$$+ \frac{q_i q_j}{4\pi\varepsilon_0 r_{ii}}$$

$$(1)$$

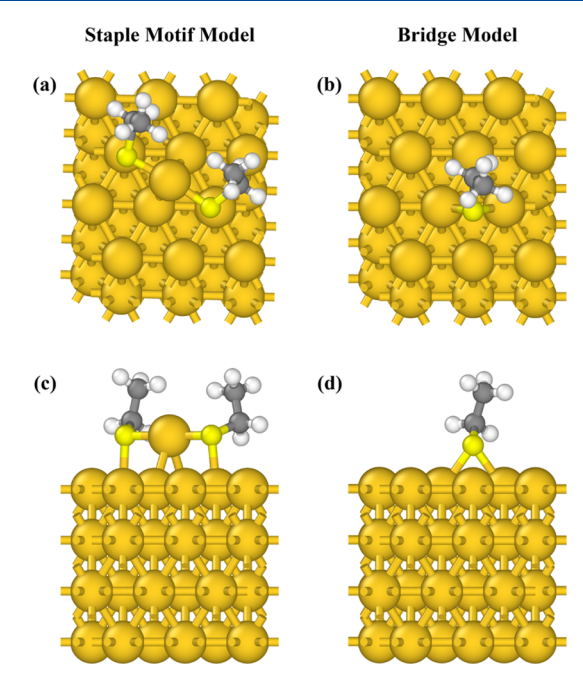
where the first three terms refer to the bonded interactions, namely, the bond, angle, and torsion interactions.  $K_b$  and  $K_\theta$  are corresponding force constants for bonds and angles;  $r_0$  and  $\theta_0$  are the equilibrium bond length and angle from DFT-based optimized configurations, respectively.  $K_n$  is the force constant for torsions.  $\phi$  is the dihedral angle, and the phase offset  $\gamma$  takes values of  $0^{\circ}$  or  $180^{\circ}$ . The latter two terms represent the nonbonded interactions, that is, van der Waals (vdW) and electrostatic interactions, which were described using the Lennard-Jones (L-J) 12-6 potential and the Coulomb's law, respectively. The Lorenz-Berthelot mixing rule was employed to calculate the vdW interactions between two different atoms. In the present study, the Au and S atoms were considered as uncharged particles, and their L-J parameters are taken from the paper by Pradip and coworkers,<sup>27</sup> while the optimized potential for liquid simulations (OPLS) all-atom force field<sup>36</sup> is used to describe interactions within the SAMs. Such force field has been widely employed to investigate the behaviors of the SAMs on the defect-free gold substrate, <sup>28,37-41</sup> as well as the SAMs-protected gold nanocluster. <sup>42,43</sup> The vdW and charge parameters used in this study are listed in Table 1.

Table 1. L-J Parameters and Partial Atomic Charges Used in This Work

atom type	$\sigma$ (Å)	arepsilon (kcal/mol)	q (e)
Au	2.934	0.039	0.000
S	3.550	0.250	0.000
$C(CH_2)$	3.500	0.066	-0.120
$C(CH_3)$	3.500	0.066	-0.180
$H(CH_2, CH_3)$	2.500	0.030	0.060

Previous studies reported a few potential functions to describe the Au–S interface, including the Gupta potential, <sup>22</sup> the pairwise L–J potential, <sup>44,45</sup> the pairwise Morse potential, <sup>46</sup> the bond-order Morse-like potential, <sup>47</sup> and ReaxFF potential. <sup>48,49</sup> In this work, we adopt the force field function form of eq 1, which has been widely implemented in numerous MD simulation packages with extensively available force field parameters for molecules and structures. Therefore, developing parameters with this form would facilitate us to study thiolate SAM interactions with other molecules in the future.

**2.3. Force Field Parameterization.** It is worth noting that despite the number of MD simulation studies of SAM systems in the literature, there is a very limited discussion of force field parameters to SAM's bonded interactions. A common practice is to either fix the Au—S bond or set relevant force constants as zero. In recent studies, it has been reported that the Au—S interface plays a key role in determining the surface properties of SAMs. Therefore, keeping the Au—S configuration rigid during the MD simulation will significantly hinder the study of interfacial SAMs. This also justifies the use of two models in the present work. As shown in Figure 1, for the staple motif model, the Au adatom, which is bonded with two S atoms atop the substrate, locates at the bridge site of the substrate; for the bridge



**Figure 1.** Top view (upper panel) and side view (lower panel) of the optimized structures for the staple motif (a,c) and the bridge (b,d) models. Color code: Au, gold; S, yellow; C, gray; and H, white.

model, the S atom resides at the bridge site of the substrate with the ethyl group pointing toward the hcp hollow site.

The force constants of bonds  $(K_b)$  and angles  $(K_\theta)$  can be obtained by fitting the force field parameters to reproduce the characteristic vibrational frequency. 50-52 For the two Au-S interface models considered here, no experimental spectrum data are available. Therefore, we first carried out DFT calculations to obtain vibrational modes and frequencies. Those results are then used as the reference for the following MD fitting calculations with the Tinker package. 55 The MINIMIZE and VIBRATE modules of Tinker were used to analyze the vibrational modes and frequencies. The force field explorer of Tinker and the Jmol<sup>54</sup> package are adopted to visualize the vibrational modes from MD and DFT, respectively.  $K_b$  and  $K_{\theta}$  are fitted until the spectra obtained from MD simulations agree with the results from DFT calculations. As for the torsion terms, see the illustration in Figure S1 of the Supporting Information 1, a different method was employed to optimize force constants: (a) first, DFT calculations were performed to obtain the torsion energy profile as a function of dihedral angles, which vary from 0 to 360° with an interval of 10° (unless specified differently). For each configuration, the geometry was optimized via DFT to obtain the total energy of the system, with the target dihedral angle and the substrate held rigid. (b) Second, the optimized configuration from DFT was used to obtain the total energy of the system via MD simulation, through the ANALYZE module of the Tinker package. (c) Finally, the force constant for the torsion term is obtained by tuning the corresponding parameters in eq 1, so that the torsion energy profile from MD agrees well with that from DFT calculations. In Supporting Information 2, we provide a detailed tutorial with reference files to show how to develop the force field parameters for bond, angle, and torsional terms considered in the present study.

#### 3. RESULTS AND DISCUSSION

**3.1. Force Field Parameters.** *3.1.1. Vibrational Frequency of Bonds and Angles.* Table 2 displays the vibrational frequencies of various modes obtained from both MD and DFT calculations. Generally, the vibrational frequencies from the staple motif and bridge models are in the range of 150–400 cm<sup>-1</sup>, which is in a good agreement with other theoretical

Table 2. Typical Vibrational Frequency of Various Modes of Staple Motif and Bridge Models<sup>a</sup>

model	mode	DFT (cm <sup>-1</sup> )	MD (cm <sup>-1</sup> )	Irelative differencel (cm <sup>-1</sup> )
staple motif model	Au(s)-S(m)	170.2	164.9	5.3
	Au(a)-S(m)	315.6	319.1	3.5
	Au(s)-S(m)-C	163.2	176.2	13.0
	Au(a)-S(m)-C	361.1	361.1	0.0
	Au(s)-S(m)-Au(a)	311.5	303.7	7.8
	S(m)-Au(a)-S(m)	191.4	188.5	2.9
	Au(s)-S(b)	168.4	167.0	1.4
Bridge model	Au(s)-S(b)-C	122.9	120.5	2.4
	Au(s)-S(b)-Au(s)	335.2	339.1	3.9

 $^a$ The atom notations in the table below are listed in Figure S1 of the Supporting Information 1.

and experimental measurements.  $^{6,55-57}$  Specifically, in the staple motif model, the Au–S stretching frequencies are 164.9 and 319.1 cm<sup>-1</sup> from MD, whereas 170.2 and 315.6 cm<sup>-1</sup> from DFT. The former is from the vertical Au–S stretching mode, while the latter is from the horizontal Au–S stretching mode. The two calculated vibration bands (both MD and DFT) agree with the radial and tangential Au–S stretching modes of the thiolate/Au nanocluster system.  $^{6,55-57}$  Furthermore, our results also agree with the previous studies that Au–S vibration bands are between 170 and  $\sim$ 350 cm<sup>-1</sup>.  $^{55}$ 

In addition, DFT calculations reveal that the Au–S–C bending mode has two bands at 163.2 and 361.1 cm<sup>-1</sup>. Considering the MD results of 176.2 and 361.1 cm<sup>-1</sup> and the satisfactory agreement between MD and DFT, the fitted force field parameters provide a good description of the system. In addition, the lower band from MD (176.2 cm<sup>-1</sup>) also agrees with the Raman spectrum of the Au–S–C bending mode, ~175–210 cm<sup>-1</sup>. We note that prior studies pointed out that this band is sensitive to the staple type, <sup>55,57</sup> indicating that the slightly higher band from the MD calculation might be attributed to the SAM model we use. For other modes of the staple motif model, there is also a satisfactory agreement between the MD and DFT calculations, as listed in Table 2.

As for the bridge model, no experimental spectrum data are available for the Au-S interface. Thus, the vibrational frequencies of various modes in the bridge model were assigned with reference to the staple motif model. The results in Table 2 show that the vibrational frequency of the Au(s)-S(b) stretching mode is 167.0 cm<sup>-1</sup> (MD)/168.4 cm<sup>-1</sup> (DFT), which is close to the counterpart of the tangential Au-S stretching mode. Moreover, for both Au(s)-S(b)-C and Au(s)-S(b)-Au(s) bending modes, the MD and DFT calculation results agree quite well, with a deviation of less than 4 cm<sup>-1</sup>. It is worth noting that the vibrational frequencies of the two modes are distinguishable from those of the staple motif model, which is due to the difference of their local structures. Hereto, the relative difference results in Table 2 clearly show that the MD can provide a good prediction for the vibrational motions of bonds and angles at the Au-S interface with both staple motif and bridge models. This means the proposed force field is capable of describing the interactions at the Au-S interface with distinct models. Based on the aforementioned MD/DFT comparisons, the obtained force

constants for bonds and angles are summarized in Tables 3 and 4

Table 3. Bond Stretching Potential Parameters for Staple Motif and Bridge Models

model	bond	$r_0$ (Å)	$K_{\rm b}~({\rm kcal/mol\cdot \AA^2})$
staple motif model	Au(s)-S(m)	2.517	45.0
	Au(a)-S(m)	2.318	100.0
Bridge model	Au(s)-S(b)	2.505	9.0

Table 4. Angle Bending Potential Parameters for Staple Motif and Bridge Models

	angle	$\theta_0  (\mathrm{deg})$	$(\text{kcal/mol·rad}^2)$
staple motif model	Au(s)-S(m)-C	105.9	10.0
	Au(a)-S(m)-C	105.8	60.0
	Au(s)-S(m)-Au(a)	93.8	50.0
	S(m)-Au(a)-S(m)	174.7	90.0
Bridge model	Au(s)-S(b)-C	111.8	37.0
	Au(s)-S(b)-Au(s)	72.7	49.0

3.1.2. Energy Profile of Dihedral Angles. The complete energy profiles for Au(s)-S(m)-C-C, Au(a)-S(m)-C-C, Au(s)-S(m)-C-H, and Au(a)-S(m)-C-H torsion terms

are listed in Figures S2-S5 for the staple motif model. The energy profile is constructed using a two-step process: first, the structure is optimized via DFT to obtain the configuration with the lowest energy; second, the energy profile is calculated by manually changing the dihedral angle, and the energy difference  $(\Delta E)$  is recorded with respect to the configuration with the lowest energy. From those energy profiles, we evaluate whether or not the fitted dihedral force field parameters reproduce DFT results. As shown in Figure 2a, when the Au(a)-S(m)-C-C torsion is in the range of  $30-100^{\circ}$ , there is a satisfactory match between the MD and DFT calculations, with an energy difference of less than 0.08 kcal/mol. It is worth noting that beyond the equilibrium range of the dihedral angle, the energy profile from MD starts to deviate from that of the DFT calculation, with a maximum deviation of about 39 kcal/ mol (see Figure S2). This larger deviation comes from the configuration, see Figure S6, when the terminal CH3 group of the thiolate is significantly departing from the equilibrium position and pointing toward the substrate. We argue that such configuration could hardly exist in reality, and a careful check on the DFT dispersion interaction correction is probably also needed, if this is the configuration of interest. To the purpose of this work, we only focus on dihedral angles near their equilibrium values.

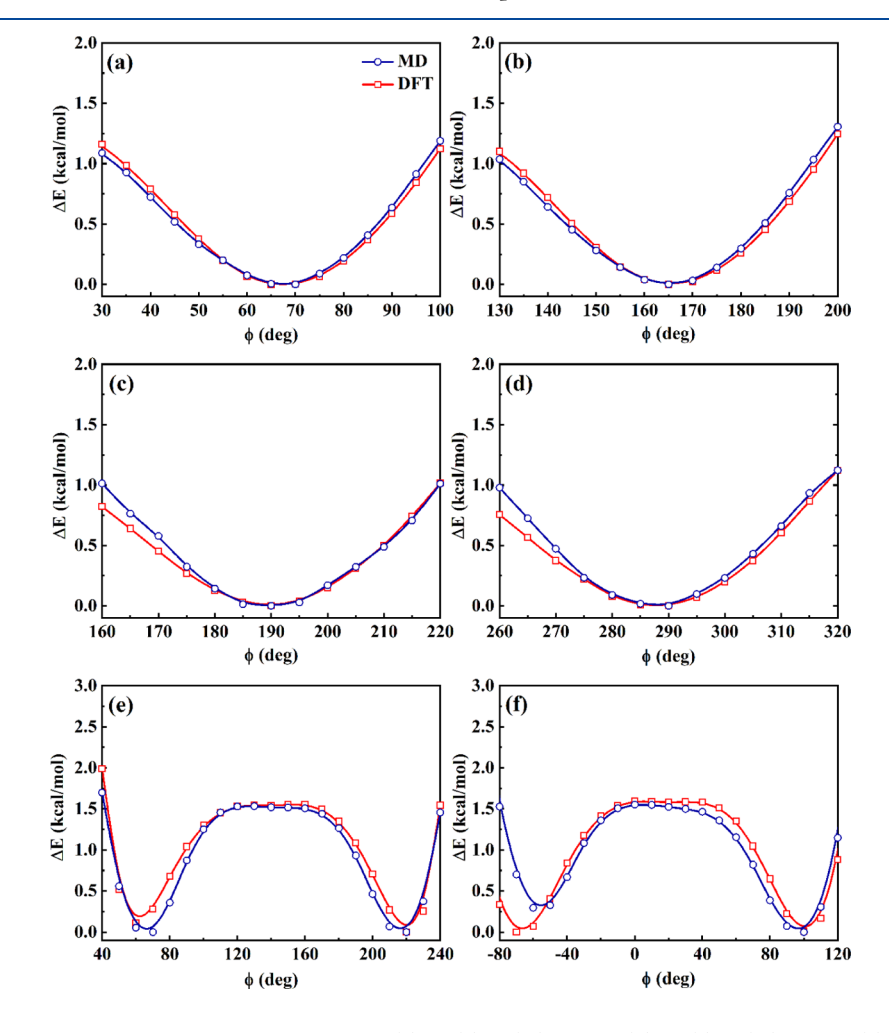


Figure 2. Torsion energy profiles from MD and DFT calculations: (a) Au(a)-S(m)-C-C, (b) Au(s)-S(m)-C-C, (c) Au(a)-S(m)-C-H, (d) Au(s)-S(m)-C-H of the staple motif model; (e) Au(s)-S(b)-C-C and (f) Au(s)-S(b)-C-H of the bridge model. Note: A small interval of  $S^{\circ}$  was used around the equilibrium dihedral value.

Table 5. Torsion Parameters for Both Staple Motif and Bridge Models

	torsions	$K_1$ (kcal/mol)	$K_2$ (kcal/mol)	$K_3$ (kcal/mol)	K <sub>4</sub> (kcal/mol)
staple motif model	Au(s)-S(m)-C-C	2.50	0.00	0.00	0.00
	Au(a)-S(m)-C-C	0.00	0.00	0.95	0.00
	Au(s)-S(m)-C-H	0.00	0.00	0.30	0.00
	Au(a)-S(m)-C-H	1.60	0.00	0.00	0.00
Bridge model	Au(s)-S(b)-C-C	2.0	4.45	2.20	0.70
	Au(s)-S(b)-C-H	0.20	0.10	0.20 <sup>a</sup>	0.10
arri i a	1.1. ( . ( ) 6(1 )	G 11 11 1 1 1 1 1 1 1 1 1 1 1 1 1 1 1 1	1000		

<sup>a</sup>The phase offset  $\gamma$  in the third term for Au(s)–S(b)–C–H dihedral angle is 180°.

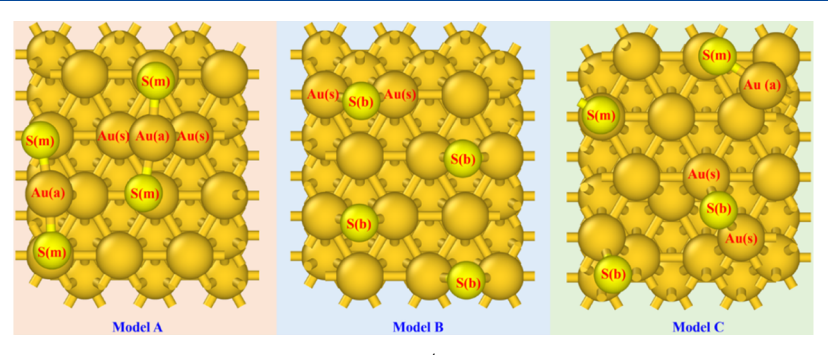


Figure 3. Atomistic structures for three Au–S interface models with a  $(2\sqrt{3} \times 3)$  unit cell including four  $C_{10}S$  thiolate molecules on the Au(111) surface. Note: the C and H atoms are not shown for clarity. Au(s), Au(a), S(m), and S(b) correspond to the Au atom in the substrate, Au adatom, S atom in the staple motif, and S atom in the bridge model.

For the Au(s)-S(m)-C-C torsion term, it is clear from Figure 2b that, in the interested range of  $130-200^\circ$ , the results from MD and DFT agree well with each other, with the energy variation smaller than 0.09 kcal/mol. When it comes to Au(a)-S(m)-C-H and Au(s)-S(m)-C-H, the complete energy profiles from MD simulation (see respectively Figures S4 and S5) exhibit a larger deviation of 7.13 and 6.26 kcal/mol, with respect to corresponding DFT calculations. Similar to the aforementioned discussion, when the studied dihedral angle changes around the equilibrium value, both energy profiles provide a satisfactory match between MD and DFT, see Figure 2c,d. The maximal energy variation is about 0.21 and 0.24 kcal/mol, respectively.

For the bridge model, there are totally two Au(s)-S(b)-C-C and four Au(s)-S(b)-C-H terms. One term of each dihedral angle was considered in this work, see the notations in Figure S1. As shown in Figures S7 and S8, the complete energy profiles for Au(s)-S(b)-C-C and Au(s)-S(b)-C-H from DFT calculations are satisfactorily reproduced by MD simulations, with a maximal energy deviation of around 14.88 and 5.49 kcal/mol, respectively. For the dihedral angle near the equilibrium value, as displayed in Figure 2e, for the Au(s)-S(b)-C-C dihedral angle of  $40-240^{\circ}$ , the energy profile from MD shows an excellent match with the DFT data, with the energy difference less than 0.35 kcal/mol. In the case of the Au(s)-S(b)-C-H dihedral angle of  $-60-120^{\circ}$ , Figure 2f demonstrates that the torsion energy profiles in that range have a good match between MD and DFT calculations, with the energy difference less than 0.3 kcal/mol. We want to note that for the Au(111) surface with a  $(2\sqrt{3} \times 3)$  unit cell of four AT molecules, the alkane chain could hardly reach the tilted configuration, as shown in Figure S9. The steric hindrance from other chains, particularly in the case of the AT molecule with a long alkane chain, will prevent that tilted configuration. The fitting results are available in Table 5 for both staple motif and bridge models.

#### 4. FORCE FIELD VALIDATION

4.1. Bonds and Angles of  $C_{10}S$  Thiolate/Au(111). To evaluate the newly fitted force field parameters, MD simulations were designed with the Tinker package<sup>53</sup> for three Au-S interface models with a  $(2\sqrt{3} \times 3)$  unit cell, having four  $C_{10}S$  thiolate molecules on the Au(111) surface. The systems are illustrated in Figure 3, and the initial configurations are available from Figures S10-S12. The periodic boundary conditions were applied in all three directions with a vacuum of 6.0 nm above the SAMs surface in the z-direction to avoid the interactions between periodic images. Each MD simulation was performed in the canonical (NVT) ensemble. The temperature was set to be 300 K, which is maintained using the Berendsen algorithm with a coupling coefficient of 0.1 ps. The velocity-Verlet algorithm was used to integrate Newton's equation of motion with a time step of 1.0 fs. A cutoff of 1.0 nm was applied for the nonbonded interactions, and the long-range electrostatic interactions were treated with the particle mesh Ewald method. 58 The total simulation time for each model was 10.0 ns, where the first 5.0 ns was for equilibrium and the latter 5.0 ns was for data analysis with the trajectory being updated every 100 steps. Meanwhile, for comparison with the MD simulations, ab-initio molecular dynamics (AIMD) calculations were also performed with the VASP package of MedeA for the three models. Similar to the MD simulations, those AIMD simulations were using the NVT ensemble, and the  $\Gamma$ -point sampling of the Brillouin zone was employed. For the AIMD calculations, the time step is 1.0 fs and a calculation of 10.0 ps was carried out for each system, with the first 5.0 ps for equilibrium and the latter 5.0 ps for collecting trajectories at every time step.

We investigated the structural features of the Au–S interface by examining the atomic distances and angles from both MD and AIMD calculations. As presented in Figures 4 and 5, in model A, the bond lengths of Au(s)-S(m) and Au(a)-S(m) from AIMD are 2.519 and 2.313 Å, respectively, in excellent

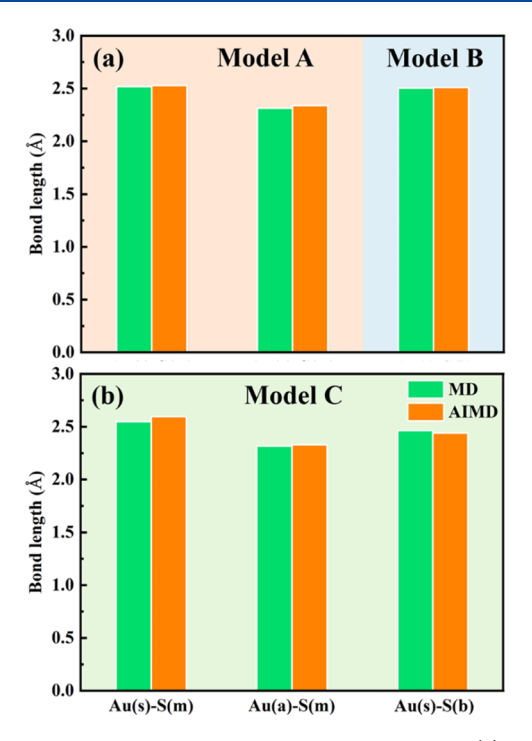
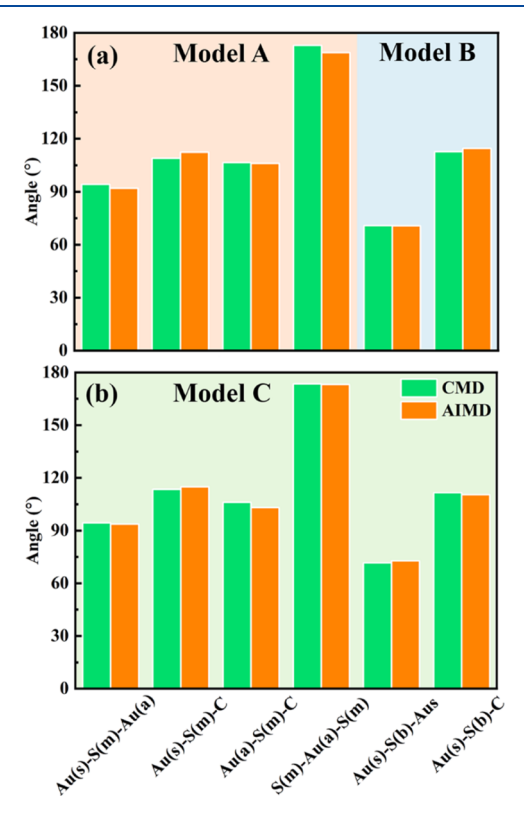


Figure 4. Average bond length for characteristic bonds in (a) model A and B and (b) model C from MD and AIMD calculations at 300 K. All standard deviations are less than  $\pm 0.05$  Å. The error bars are smaller than the symbol size, therefore not shown.



**Figure 5.** Average angle values for various angles in (a) model A and B and (b) model C from MD and AIMD calculations at 300 K. All standard deviations are less than  $\pm 1.5^{\circ}$ . The error bars are smaller than the symbol size, so they are not shown.

agreement with the MD results of 2.528 and 2.339 Å. The Au(s)-S(b) bond length in model B is only 0.005 Å shorter

than the AIMD value (2.510 Å). For model C, the Au(s)-S(m) and Au(a)-S(m) bond lengths from MD are 2.547 and 2.318 Å, respectively, while corresponding AIMD calculations predict 2.597 and 2.328 Å. The bond length of Au(s)-S(b) from MD is 0.023 Å longer than that of the AIMD value (2.442 Å).

In addition, when it comes to the angle values, there is also a good agreement between MD and AIMD calculations. Specifically, in model A, the Au(a)-S(m)-C is calculated to be 106.49° with MD, and 106.11° with AIMD. For the other three angles, namely, Au(s)-S(m)-Au(a), Au(a)-S(m)-C, and S(m)-Au(a)-S(m), the MD values are also close to the AIMD predictions, with a maximum deviation less than 4.0°. The Au(s)-S(b)-Au(s) and Au(s)-S(b)-C angles in model B with MD are 70.88 and 112.73°, respectively, while the corresponding values of 70.76 and 114.52° with AIMD calculations. In model C, the angles, for example, Au(s)-S(m)-Au(a) (94.41°), Au(a)-S(m)-C (106.09°), S(m)-CAu(a)-S(m) (173.60°), and Au(s)-S(b)-C (111.55°) from MD are slightly larger than the AIMD results. The opposite trend, namely, DFT predicting a slightly larger value than that of MD, was observed for the other two angles of Au(s)-S(m)-C and Au(s)-S(b)-Au(s). However, the absolute numerical difference between MD and AIMD is still negligible. On the other hand, it should be mentioned that the average bond length and angle measurements in Figures 4 and 5 are very close to their equilibrium values from DFT optimized configurations. We thus conclude that the newly developed force field parameters are satisfactorily predicting structural features of all three Au-S interface models in Figure 3.

4.2. Alkane Chain Distribution of C<sub>10</sub>S Thiolate/ Au(111). The density distribution was also calculated of C atoms in the alkane chain along the z-direction, as illustrated in Figure 6. The results demonstrate that for both MD and AIMD calculations, there is a well-defined distribution for the position of the first C atom near the Au(111) surface. The density profiles also reveal the formation of doublet corresponding to pairs of C atoms, while the terminal C atom of the CH<sub>3</sub> group shows an isolated peak distribution. In addition, the new force field seems to provide a better prediction to model B, regarding the C atom distributions. Whereas, in model A, when C atoms are away from the Au(111) surface, for example, starting with the 5th Carbon atom of the alkane chain, DFT predicts a larger C-surface distance than that from MD. This is probably attributed to vdW interactions from MD and AIMD calculations. 59 We also note that there is some deviation to the density intensity predicted by MD and AIMD, which is likely resulting from alkane chain flexibility at finite temperatures of AIMD calculations. For model C, the results in Figure 6c show that some carbon peak positions from AIMD calculation were not satisfactorily reproduced by MD simulations. Compared with the unique staple motif in model A and the bridge unit in model B, model C has a combination of staple motif and bridge units, which makes the model a more complex one. Therefore, to have a more detailed comparison between MD and AIMD data, the integrated density distribution profiles in Figure 6c have been divided into four individual parts, as shown in Figure S13 of the Supporting Information 1. For molecules 1 and 2 in the staple motif unit (see the notations of the four C<sub>10</sub>S molecules in the model C in Figure S14 of the Supporting Information 1), the density distribution profiles show a good agreement between MD and AIMD results for the first four C atoms, after which the MD results start to deviate

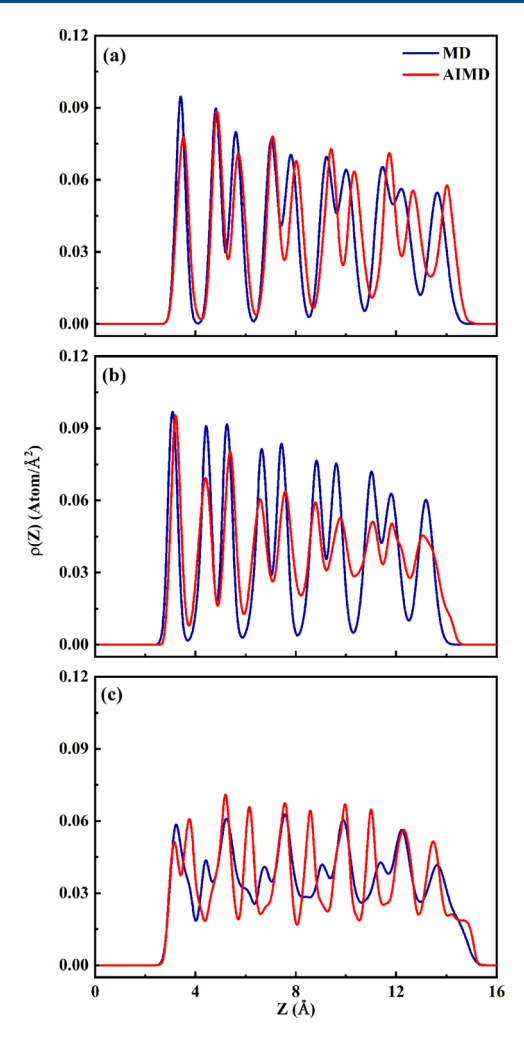


**Figure 6.** Density distributions of the C atoms in the alkane chain along the z-direction for (a) model A, (b) model B, and (c) model C at 300.0 K.

from those from AIMD, especially in the case of molecule 1. For the two molecules in the bridge unit, the density distribution profiles of molecule 3 from MD agree well with the AIMD results. However, the distribution results of molecule 4 in Figure S13d show that the MD simulation has good description for the positions of the odd-numbered C atoms, whereas the results of the even-numbered C atoms (except the terminal methyl group) exhibit noticeable deviations from AIMD. This is primarily due to the fact that the vacancy defect is not included in the force field fitting

process. Therefore, those bonded interactions in molecule 4 might shift the locations of C atoms from what were predicted in AIMD calculations. In addition, it can be concluded that the obtained force field in this study can provide a good description for the pristine Au—S interface models with unique staple motif or bridge units. However, more force field training efforts will be required to satisfactorily describe the defective Au—S interface model with both the vacancy and adatom. The exclusion of the surface vacancy defect during the force field training is responsible for the potential failure to predict vertical locations of C atoms in the bridge SAM molecules.

4.3. Tilt Angle, Azimuthal Angle, and Film Thickness of C<sub>10</sub>S Thiolate/Au(111). Lastly, other critical properties of the C<sub>10</sub>S thiolate, including the tilt angle, the azimuthal angle, and the film thickness, are also explored by both MD and AIMD calculations. As illustrated in Figure S15, the tilt angle to the alkane chain was computed as the angle formed between the surface normal and the line passing through the S atom and the centroid of each chain. In model A, the tilt angle from MD  $(36.13 \pm 0.02^{\circ})$  is slightly larger than that predicted by AIMD calculation (34.32  $\pm$  2.48°). Such a difference is likely due to the peak position difference of the terminal CH<sub>3</sub> group, as shown in Figure 6a. For models B and C, MD and AIMD agree well about the tilt angle of C<sub>10</sub>S, with a maximum variation of about 2°. Accordingly, the azimuthal angle is defined as the angle formed between the projection on the x-y plane of the lines passing through the S atom and the centroid of the alkane chain and the unit vector along the x-direction. The results in Table 6 show that, for the studied three models, the azimuthal angle from MD is in a satisfactory agreement with the AIMD results, with a maximum deviation of less than 5°. Finally, the film thickness is estimated by calculating the distance from the terminal CH3 group to the gold substrate. The calculations reveal that MD and DFT have an excellent agreement on the film thickness, with a difference within 0.3 Å for three Au-S interface models. Overall, the results in Table 6 demonstrate a good agreement between the MD and AIMD results in tilt angle, azimuthal angle, and film thickness for all three models considered in this study. A detailed comparison among these models reveals that the MD simulation has a better description for the defective model C in the tilt angle and film thickness, but for the pristine model B in azimuthal angle. Based on above discussion, we conclude that the fitted force field parameters provide an accurate description of structural properties of C<sub>10</sub>S SAMs at the Au(111) surface with different local environments at the Au-S interface.

Table 6. Average Tilt Angle, Azimuthal Angle, and Film Thickness for the Alkane Chains in Model A, B, and C from MD and AIMD Calculations at 300 K

	Item	tilt angle (deg)	azimuthal angle (deg)	film thickness (Å)		
model A	MD	MD $36.13 \pm 0.02$		$13.55 \pm 0.01$		
	AIMD	$34.32 \pm 2.48$	$9.99 \pm 4.12$	$13.78 \pm 0.30$		
	Irelative differencel	$1.81 \pm 2.46$	$4.55 \pm 3.71$	$0.23 \pm 0.29$		
model B	MD	$35.41 \pm 0.05$	$116.01 \pm 0.10$	$13.07 \pm 0.01$		
	AIMD	$33.23 \pm 2.28$	$117.10 \pm 6.20$	$13.28 \pm 0.30$		
	Irelative differencel	$2.18 \pm 2.23$	$1.09 \pm 6.10$	$0.21 \pm 0.29$		
model C	MD	$30.72 \pm 0.07$	$56.11 \pm 0.19$	$13.81 \pm 0.01$		
	AIMD	$30.50 \pm 4.18$	$60.88 \pm 4.97$	$13.86 \pm 0.39$		
	Irelative differencel	$0.22 \pm 4.11$	$4.77 \pm 4.18$	$0.07 \pm 0.38$		

#### 5. CONCLUSIONS

In the present study, periodic ab initio DFT calculations were performed to develop force field parameters to describe AT SAMs at the reconstructed Au(111) surface. The new parameters were carefully trained to reproduce the key features, including vibrational spectra and torsion energy profiles, of C2S in the bridge and staple motif units at the Au(111) surface. The nonbonded force field parameters were directly adopted from the work of Rai et al.;<sup>27</sup> while the bonded parameters were obtained by reproducing DFT calculation results with iterated MD simulations. In specific, the force constants of bonds and angles were trained by matching the vibrational spectra, while the dihedral parameters were fitted according to the torsion energy profiles. For the vibrational spectra of bonds and angles, MD and DFT agree well with each other, with a maximum deviation about 12 cm<sup>-1</sup>. Using the fitted parameters, MD simulations can reproduce the dihedral energy profiles from DFT calculations. The agreement is excellent around equilibrium dihedral angles.

In addition, the newly developed force field parameters have been also validated by performing MD simulations for three Au–S interface models by a  $(2\sqrt{3}\times3)$  unit cell with four  $C_{10}S$  SAMs. Those MD results were also compared with AIMD calculation results. Structural features, including the bond length, angle measurement, alkane carbon locations, the tilt angle, azimuthal angle, and the film thickness of the  $C_{10}S$  SAMs, have been calculated. The MD results agree well with those from DFT calculations, which demonstrates a reliability of the developed force field parameters for alkanethiolate SAMs at the reconstructed Au(111) surface.

#### ASSOCIATED CONTENT

#### Supporting Information

The Supporting Information is available free of charge at https://pubs.acs.org/doi/10.1021/acs.langmuir.0c00530.

Atom notation for the torsion terms; complete energy profiles for considered torsion terms; typical configurations in staple motif and bridge models; initial configurations of MD simulations for three Au–S interface models; individual density distribution of the C atoms in model C (PDF)

Detailed fitting procedures used to develop the force constants for bond, angle, and torsional terms (PDF) (ZIP)

#### AUTHOR INFORMATION

#### **Corresponding Author**

Liangliang Huang — School of Chemical, Biological and Materials Engineering, University of Oklahoma, Norman, Oklahoma 73019, United States; orcid.org/0000-0003-2358-9375; Email: HLL@ou.edu

#### **Authors**

**Guobing Zhou** — School of Chemical, Biological and Materials Engineering, University of Oklahoma, Norman, Oklahoma 73019, United States

Chang Liu — State Key Laboratory of Materials-Oriented Chemical Engineering, Nanjing Tech University, Nanjing 210009, China

**Lloyd A. Bumm** – Homer L. Dodge Department of Physics and Astronomy, University of Oklahoma, Norman, Oklahoma 73019, United States; orcid.org/0000-0003-2301-8193

Complete contact information is available at: https://pubs.acs.org/10.1021/acs.langmuir.0c00530

#### Notes

The authors declare no competing financial interest.

#### ACKNOWLEDGMENTS

G.Z., L.A.B., and L.H. acknowledge the U.S. National Science Foundation (NSF) for the support through Grant CHE-1710102. C.L. acknowledges the support from the Natural Science Foundation of China (21878143). We are very pleased to thank the OU Supercomputing Center for Education & Research (OSCER) at the University of Oklahoma and the High-Performance Computing Center of Nanjing Tech University for their dedicated support.

#### REFERENCES

- (1) Love, J. C.; Estroff, L. A.; Kriebel, J. K.; Nuzzo, R. G.; Whitesides, G. M. Self-Assembled Monolayers of Thiolates on Metals as a Form of Nanotechnology. *Chem. Rev.* **2005**, *105*, 1103–1170.
- (2) Vericat, C.; Vela, M. E.; Corthey, G.; Pensa, E.; Cortés, E.; Fonticelli, M. H.; Ibañez, F.; Benitez, G. E.; Carro, P.; Salvarezza, R. C. Self-Assembled Monolayers of Thiolates on Metals: A Review Article on Sulfur-Metal Chemistry and Surface Structures. *RSC Adv.* **2014**, *4*, 27730–27754.
- (3) Ulman, A. Formation and Structure of Self-Assembled Monolayers. Chem. Rev. 1996, 96, 1533–1554.
- (4) Vericat, C.; Vela, M. E.; Benitez, G.; Carro, P.; Salvarezza, R. C. Self-Assembled Monolayers of Thiols and Dithiols on Gold: New Challenges for a Well-Known System. *Chem. Soc. Rev.* **2010**, 39, 1805–1834.
- (5) Häkkinen, H. The Gold-Sulfur Interface at the Nanoscale. *Nat. Chem.* **2012**, *4*, 443–455.
- (6) Bürgi, T. Properties of the Gold-Sulphur Interface: From Self-Assembled Monolayers to Clusters. *Nanoscale* **2015**, *7*, 15553–15567.
- (7) Pensa, E.; Cortés, E.; Corthey, G.; Carro, P.; Vericat, C.; Fonticelli, M. H.; Benítez, G.; Rubert, A. A.; Salvarezza, R. C. The Chemistry of the Sulfur–Gold Interface: In Search of a Unified Model. *Acc. Chem. Res.* **2012**, *45*, 1183–1192.
- (8) Akkerman, H. B.; Blom, P. W. M.; de Leeuw, D. M.; de Boer, B. Towards Molecular Electronics with Large-Area Molecular Junctions. *Nature* **2006**, *441*, 69–72.
- (9) Chaki, N. K.; Vijayamohanan, K. Self-Assembled Monolayers as a Tunable Platform for Biosensor Applications. *Biosens. Bioelectron.* **2002**, *17*, 1–12.
- (10) Daniel, M.-C.; Astruc, D. Gold Nanoparticles: Assembly, Supramolecular Chemistry, Quantum-Size-Related Properties, and Applications toward Biology, Catalysis, and Nanotechnology. *Chem. Rev.* **2004**, *104*, 293–346.
- (11) Giljohann, D. A.; Seferos, D. S.; Daniel, W. L.; Massich, M. D.; Patel, P. C.; Mirkin, C. A. Gold Nanoparticles for Biology and Medicine. *Angew. Chem., Int. Ed.* **2010**, *49*, 3280–3294.
- (12) Bigelow, W. C.; Pickett, D. L.; Zisman, W. A. Oleophobic Monolayers .1. Films Adsorbed from Solution in Non-Polar Liquids. *J. Colloid Sci.* **1946**, *1*, 513–538.
- (13) Vericat, C.; Vela, M. E.; Benitez, G. A.; Gago, J. A. M.; Torrelles, X.; Salvarezza, R. C. Surface Characterization of Sulfur and Alkanethiol Self-Assembled Monolayers on Au(111). *J. Phys.: Condens. Matter* **2006**, *18*, R867–R900.
- (14) Vericat, C.; Vela, M. E.; Salvarezza, R. C. Self-Assembled Monolayers of Alkanethiols on Au(111): Surface Structures, Defects and Dynamics. *Phys. Chem. Chem. Phys.* **2005**, *7*, 3258–3268.
- (15) Cossaro, A.; Mazzarello, R.; Rousseau, R.; Casalis, L.; Verdini, A.; Kohlmeyer, A.; Floreano, L.; Scandolo, S.; Morgante, A.; Klein, M. L.; Scoles, G. X-Ray Diffraction and Computation Yield the Structure of Alkanethiols on Gold(111). *Science* **2008**, 321, 943–946.

- (16) Nuzzo, R. G.; Zegarski, B. R.; Dubois, L. H. Fundamental-Studies of the Chemisorption of Organosulfur Compounds on Au(111) Implications for Molecular Self-Assembly on Gold Surfaces. *J. Am. Chem. Soc.* **1987**, *109*, 733–740.
- (17) Hayashi, T.; Morikawa, Y.; Nozoye, H. Adsorption State of Dimethyl Disulfide on Au(111): Evidence for Adsorption as Thiolate at the Bridge Site. *J. Chem. Phys.* **2001**, *114*, 7615–7621.
- (18) Vargas, M. C.; Giannozzi, P.; Selloni, A.; Scoles, G. Coverage-Dependent Adsorption of Ch3s and (Ch3s)(2) on Au(111): A Density Functional Theory Study. *J. Phys. Chem. B* **2001**, *105*, 9509–9513
- (19) Gottschalck, J.; Hammer, B. A Density Functional Theory Study of the Adsorption of Sulfur, Mercapto, and Methylthiolate on Au(111). *J. Chem. Phys.* **2002**, *116*, 784–790.
- (20) Morikawa, Y.; Liew, C. C.; Nozoye, H. Methylthiolate Induced Vacancy Formation on Au(111): A Density Functional Theoretical Study. Surf. Sci. 2002, 514, 389–393.
- (21) Molina, L. M.; Hammer, B. Theoretical Study of Thiol-Induced Reconstructions on the Au(111) Surface. *Chem. Phys. Lett.* **2002**, *360*, 264–271.
- (22) Longo, G. S.; Bhattacharya, S. K.; Scandolo, S. A Molecular Dynamics Study of the Role of Adatoms in Sams of Methylthiolate on Au(111): A New Force Field Parameterized from Ab Initio Calculations. *J. Phys. Chem. C* **2012**, *116*, 14883–14891.
- (23) Chaudhuri, A.; Lerotholi, T. J.; Jackson, D. C.; Woodruff, D. P.; Jones, R. G. (2 Root 3x3)Rect. Phase of Alkylthiolate Self-Assembled Monolayers on Au(111): A Symmetry-Constrained Structural Solution. *Phys. Rev. B: Condens. Matter Mater. Phys.* **2009**, *79*, 195439.
- (24) Wang, J.-g.; Selloni, A. The C(4 X 2) Structure of Short-and Intermediate-Chain Length Alkanethiolate Monolayers on Au(111): A Dft Study. *J. Phys. Chem. C* **2007**, *111*, 12149–12151.
- (25) Torres, E.; Biedermann, P. U.; Blumenau, A. T. The Role of Gold Adatoms in Self-Assembled Monolayers of Thiol on Au(111). *Int. J. Quantum Chem.* **2009**, *109*, 3466–3472.
- (26) Wang, Y.; Chi, Q.; Hush, N. S.; Reimers, J. R.; Zhang, J.; Ulstrup, J. Scanning Tunneling Microscopic Observation of Adatom-Mediated Motifs on Gold-Thiol Self-Assembled Monolayers at High Coverage. *J. Phys. Chem. C* **2009**, *113*, 19601–19608.
- (27) Rai, B.; Sathish, P.; Malhotra, C. P.; Pradip; Ayappa, K. G. Molecular Dynamic Simulations of Self-Assembled Alkylthiolate Monolayers on an Au(111) Surface. *Langmuir* **2004**, *20*, 3138–3144.
- (28) Devi, J. M. A Simulation Study on the Thermal and Wetting Behavior of Alkane Thiol Sam on Gold (111) Surface. *Prog. Nat. Sci.* **2014**, 24, 405–411.
- (29) Xu, Z.; Song, K.; Yuan, S.-L.; Liu, C.-B. Microscopic Wetting of Self-Assembled Mono Layers with Different Surfaces: A Combined Molecular Dynamics and Quantum Mechanics Study. *Langmuir* **2011**, 27, 8611–8620.
- (30) Tobias, D. J.; Mar, W.; Blasie, J. K.; Klein, M. L. Molecular Dynamics Simulations of a Protein on Hydrophobic and Hydrophilic Surfaces. *Biophys. J.* **1996**, *71*, 2933–2941.
- (31) Hung, S.-W.; Kikugawa, G.; Shiomi, J. Mechanism of Temperature Dependent Thermal Transport across the Interface between Self-Assembled Monolayer and Water. *J. Phys. Chem. C* **2016**, 120, 26678–26685.
- (32) Kresse, G.; Furthmüller, J. Efficient Iterative Schemes for Ab Initio Total-Energy Calculations Using a Plane-Wave Basis Set. *Phys. Rev. B: Condens. Matter Mater. Phys.* **1996**, *54*, 11169–11186.
- (33) Blöchl, P. E. Projector Augmented-Wave Method. Phys. Rev. B: Condens. Matter Mater. Phys. 1994, 50, 17953–17979.
- (34) Perdew, J. P.; Burke, K.; Ernzerhof, M. Generalized Gradient Approximation Made Simple. *Phys. Rev. Lett.* **1996**, *77*, 3865–3868.
- (35) Grimme, S.; Antony, J.; Ehrlich, S.; Krieg, H. A Consistent and Accurate Ab Initio Parametrization of Density Functional Dispersion Correction (Dft-D) for the 94 Elements H-Pu. *J. Chem. Phys.* **2010**, 132, 154104.
- (36) Jorgensen, W. L.; Maxwell, D. S.; Tirado-Rives, J. Development and Testing of the Opls All-Atom Force Field on Conformational

- Energetics and Properties of Organic Liquids. J. Am. Chem. Soc. 1996, 118, 11225—11236.
- (37) Goujon, F.; Bonal, C.; Limoges, B.; Malfreyt, P. Description of Ferrocenylalkylthiol Sams on Gold by Molecular Dynamics Simulations. *Langmuir* **2009**, 25, 9164–9172.
- (38) Goujon, F.; Bonal, C.; Limoges, B.; Malfreyt, P. Molecular Dynamics Simulations of Ferrocene-Terminated Self-Assembled Monolayers. *J. Phys. Chem. B* **2010**, *114*, 6447–6454.
- (39) Filippini, G.; Israeli, Y.; Goujon, F.; Limoges, B.; Bonal, C.; Malfreyt, P. Free Energy Calculations in Electroactive Self-Assembled Monolayers (Sams): Impact of the Chain Length on the Redox Reaction. *J. Phys. Chem. B* **2011**, *115*, 11678–11687.
- (40) Kislenko, S. A.; Nikitina, V. A.; Nazmutdinov, R. R. When Do Defectless Alkanethiol Sams in Ionic Liquids Become Penetrable? A Molecular Dynamics Study. *Phys. Chem. Chem. Phys.* **2015**, *17*, 31947–31955.
- (41) Filippini, G.; Bonal, C.; Malfreyt, P. Atomistic and Energetic Descriptions of Self-Assembled Monolayers of Differently Endgroup-Functionalized Alkanethiols Adsorbed on the Gold Substrate by Using Molecular Simulations. *Soft Matter* **2013**, *9*, 5099–5109.
- (42) Milano, G.; Santangelo, G.; Ragone, F.; Cavallo, L.; Di Matteo, A. Gold Nanoparticle/Polymer Interfaces: All Atom Structures from Molecular Dynamics Simulations. *J. Phys. Chem. C* **2011**, *115*, 15154–15163.
- (43) Munao, G.; Correa, A.; Pizzirusso, A.; Milano, G. On the Calculation of the Potential of Mean Force between Atomistic Nanoparticles. *Eur. Phys. J. E* **2018**, *41*, 38.
- (44) Yang, Z.; Li, Y.; Zhou, G.; Chen, X.; Tao, D.; Hu, N. Molecular Dynamics Simulations of Hydrogen Bond Dynamics and Far-Infrared Spectra of Hydration Water Molecules around the Mixed Monolayer-Protected Au Nanoparticle. *J. Phys. Chem. C* **2015**, *119*, 1768–1781.
- (45) Li, Y. Z.; Yang, Z.; Hu, N.; Zhou, R. F.; Chen, X. S. Insights into Hydrogen Bond Dynamics at the Interface of the Charged Monolayer-Protected Au Nanoparticle from Molecular Dynamics Simulation. *J. Chem. Phys.* **2013**, *138*, 184703.
- (46) Mahaffy, R.; Bhatia, R.; Garrison, B. J. Diffusion of a Butanethiolate Molecule on a Au{111} Surface. *J. Phys. Chem. B* **1997**, 101, 771–773.
- (47) Olmos-Asar, J. A.; Rapallo, A.; Mariscal, M. M. Development of a Semiempirical Potential for Simulations of Thiol-Gold Interfaces. Application to Thiol-Protected Gold Nanoparticles. *Phys. Chem. Chem. Phys.* **2011**, *13*, 6500–6506.
- (48) Bae, G.-T.; Aikens, C. M. Improved Reaxff Force Field Parameters for Au-S-C-H Systems. J. Phys. Chem. A 2013, 117, 10438–10446.
- (49) Järvi, T. T.; van Duin, A. C. T.; Nordlund, K.; Goddard, W. A. Development of Interatomic Reaxff Potentials for Au-S-C-H Systems. *J. Phys. Chem. A* **2011**, *115*, 10315–10322.
- (50) Wang, Y.-L.; Shah, F. U.; Glavatskih, S.; Antzutkin, O. N.; Laaksonen, A. Atomistic Insight into Orthoborate-Based Ionic Liquids: Force Field Development and Evaluation. *J. Phys. Chem. B* **2014**, *118*, 8711–8723.
- (51) Liu, Z.; Huang, S.; Wang, W. A Refined Force Field for Molecular Simulation of Imidazolium-Based Ionic Liquids. *J. Phys. Chem. B* **2004**, *108*, 12978–12989.
- (52) de Andrade, J.; Böes, E. S.; Stassen, H. Computational Study of Room Temperature Molten Salts Composed by 1-Alkyl-3-Methylimidazolium Cations-Force-Field Proposal and Validation. *J. Phys. Chem. B* **2002**, *106*, 13344–13351.
- (53) Pappu, R. V.; Hart, R. K.; Ponder, J. W. Analysis and Application of Potential Energy Smoothing and Search Methods for Global Optimization. *J. Phys. Chem. B* **1998**, *102*, 9725–9742.
- (54) Jmol: An Open-Source Java Viewer for Chemical Structures in 3d. http://www.jmol.org/. Accessed data: March 31, 2020.
- (55) Nieto-Ortega, B.; Bürgi, T. Vibrational Properties of Thiolate-Protected Gold Nanoclusters. *Acc. Chem. Res.* **2018**, *51*, 2811–2819.
- (56) Varnholt, B.; Oulevey, P.; Luber, S.; Kumara, C.; Dass, A.; Bürgi, T. Structural Information on the Au-S Interface of Thiolate-

Protected Gold Clusters: A Raman Spectroscopy Study. *J. Phys. Chem.* C **2014**, *118*, 9604–9611.

- (57) Varnholt, B.; Guberman-Pfeffer, M. J.; Oulevey, P.; Antonello, S.; Dainese, T.; Gascón, J. A.; Bürgi, T.; Maran, F. Vibrational Coupling Modulation in N-Alkanethiolate Protected Au-25(Sr)(18) (0) Clusters. J. Phys. Chem. C 2016, 120, 25378–25386.
- (58) Essmann, U.; Perera, L.; Berkowitz, M. L.; Darden, T.; Lee, H.; Pedersen, L. G. A Smooth Particle Mesh Ewald Method. *J. Chem. Phys.* **1995**, *103*, 8577–8593.
- (59) Reimers, J. R.; Ford, M. J.; Marcuccio, S. M.; Ulstrup, J.; Hush, N. S. Competition of Van Der Waals and Chemical Forces on Gold-Sulfur Surfaces and Nanoparticles. *Nat. Rev. Chem.* **2017**, *1*, 17.

# Force Field Parameter Development for the Thiolate/Defective Au (111) Interface

Guobing Zhou, a Chang Liu, b Lloyd A. Bumm, c Liangliang Huang\*a

- (a) School of Chemical, Biological and Materials Engineering, University of Oklahoma, Norman, Oklahoma 73019, United States
- (b) State Key Laboratory of Materials-Oriented Chemical Engineering, Nanjing Tech University, Nanjing 210009, China
- (c) Homer L. Dodge Department of Physics and Astronomy, University of Oklahoma, Norman, Oklahoma 73019, United States

## **Supporting Information 1**

The list of figures provided in this supporting material:

- 1. Figure S1. The notation of various atom types in the torsion terms used for the force field development in this study.
- 2. Figure S2. Complete torsion energy profiles for Au(a)-S(m)-C-C dihedral angle in the staple motif model obtained from MD and DFT calculations.
- 3. Figure S3. Complete torsion energy profiles for Au(s)-S(m)-C-C dihedral angle in the staple motif model obtained from MD and DFT calculations.
- 4. Figure S4. Complete torsion energy profiles for Au(a)-S(m)-C-H dihedral angle in the staple motif model obtained from MD and DFT calculations.
- 5. Figure S5. Complete torsion energy profiles for Au(s)-S(m)-C-H dihedral angle in the staple motif model obtained from MD and DFT calculations.
- 6. Figure S6. (a) top and (b) side views of the staple motif configuration where the dihedral angle of Au(s)-S(m)-C-C is 260°. Color code: Au, gold; S, yellow; C, gray; H, white.
- 7. Figure S7. Complete torsion energy profiles for Au(s)-S(b)-C-C in dihedral angle the bridge model obtained from MD and DFT calculations.
- 8. Figure S8. (a) Complete torsion energy profiles for Au(s)-S(b)-C-H dihedral angle in the bridge model obtained from MD and DFT calculations, (b) top and (c, d) side views of the bridge configuration where the dihedral angle of Au(s)-S(b)-C-H is -180° (180)°. Color code: Au, gold; S, yellow; C, gray; H, white.

- 9. Figure S9. (a) top and (b) side views of the bridge configuration where the dihedral angle of Au(s)-S(b)-C-H is -70 (290)°. Color code: Au, gold; S, yellow; C, gray; H, white.
- 10. Figure S10. Side views of the initial configuration for model A with the unit  $(2\sqrt{3}\times3)$  unit cell being duplicated  $5\times5$  in x and y directions, respectively. Color code: Au, gold; S, yellow; C, gray; H, white.
- 11. Figure S11. Side views of the initial configuration for model B with the unit  $(2\sqrt{3}\times3)$  unit cell being duplicated  $5\times5$  in x and y directions, respectively. Color code: Au, gold; S, yellow; C, gray; H, white.
- 12. Figure S12. Side views of the initial configuration for model C with the unit  $(2\sqrt{3}\times3)$  unit cell being duplicated  $5\times5$  in x and y directions, respectively. Color code: Au, gold; S, yellow; C, gray; H, white.
- 13. Figure S13. Density distributions of the C atoms in alkane chain along the z direction for (a) molecule 1, (b) molecule 2, (c) molecule 3, and (d) molecule 4 in model C at 200.0 K. The four molecules are denoted as M1, M2, M3, and M4 in Figure S14.
- 14. Figure S14. The notations of the four  $C_{10}S$  molecules in the model C listed in Figure 3.
- 15. Figure S15. Schematic illustrations for the vectors and angles used in this study. Note:  $\mathbf{u}_1$  is the vector passing through the S atom and the centroid of each chain;  $\mathbf{u}_2$  is the projection of vector  $\mathbf{u}_1$  in x-y plane. Tilt angle  $\boldsymbol{\alpha}$  is formed between the surface normal vector and vector  $\mathbf{u}_1$ , and the azimuthal angle  $\boldsymbol{\chi}$  is defined as the angle between vector  $\mathbf{u}_2$  and the unit vector along the x-direction.

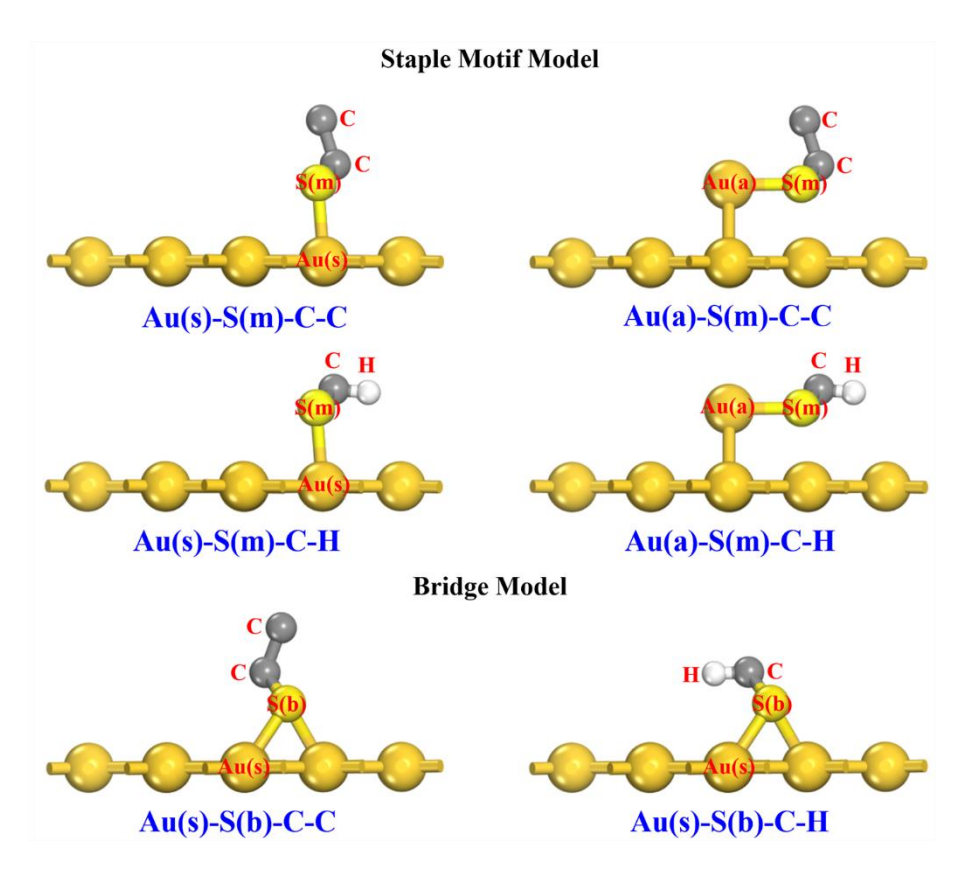


**Figure S1.** The notation of various atom types in the torsion terms used for the force field development in this study.

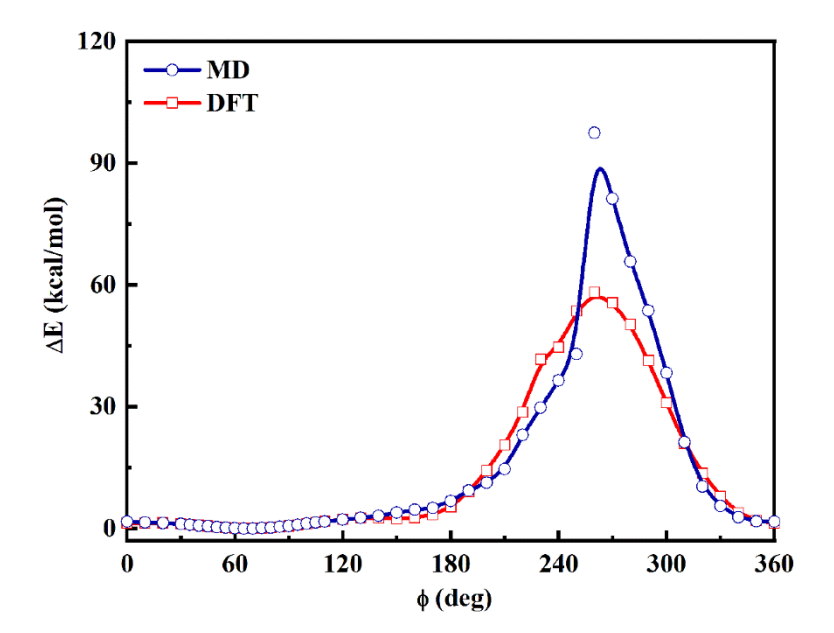


**Figure S2**. Complete torsion energy profiles for Au(a)-S(m)-C-C dihedral angle in the staple motif model obtained from MD and DFT calculations.

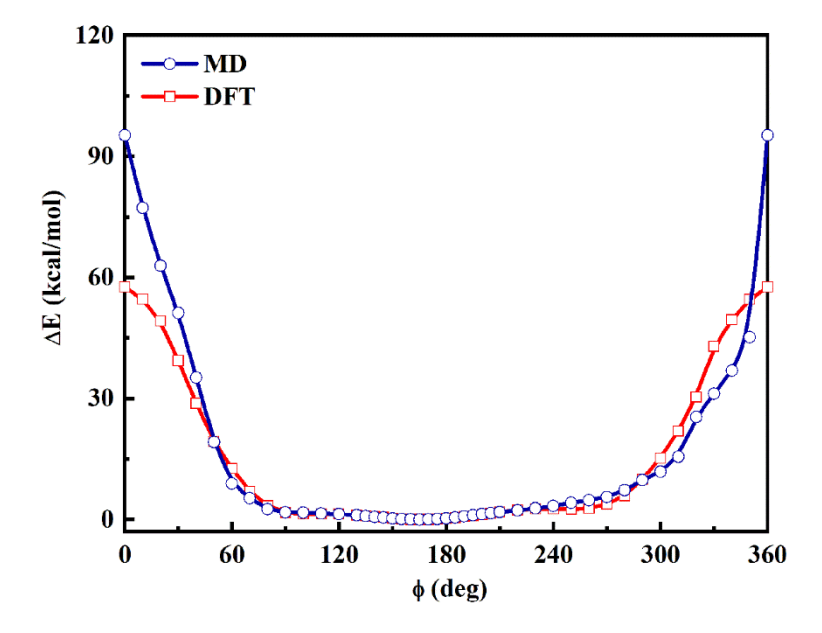


**Figure S3**. Complete torsion energy profiles for Au(s)-S(m)-C-C dihedral angle in the staple motif model obtained from MD and DFT calculations.

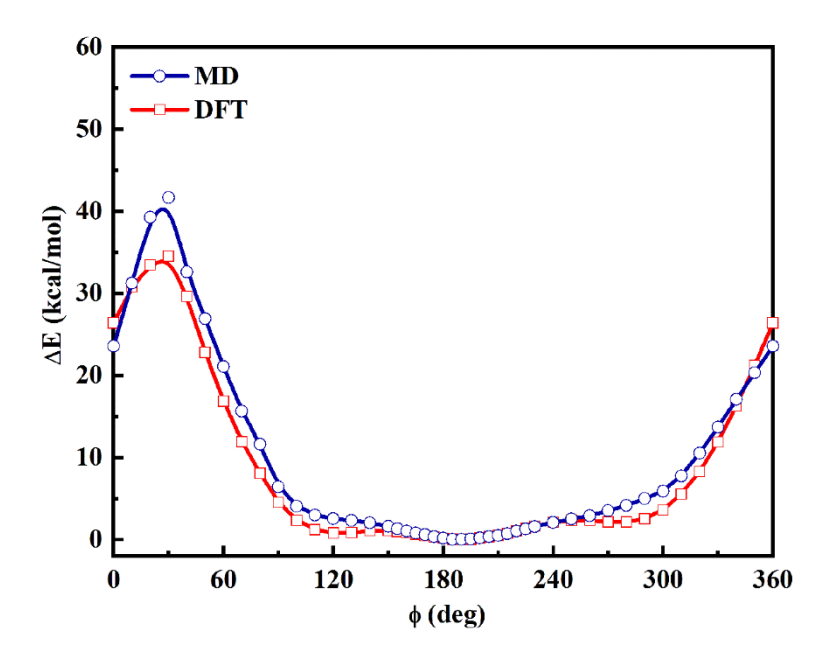


**Figure S4**. Complete torsion energy profiles for Au(a)-S(m)-C-H dihedral angle in the staple motif model obtained from MD and DFT calculations.

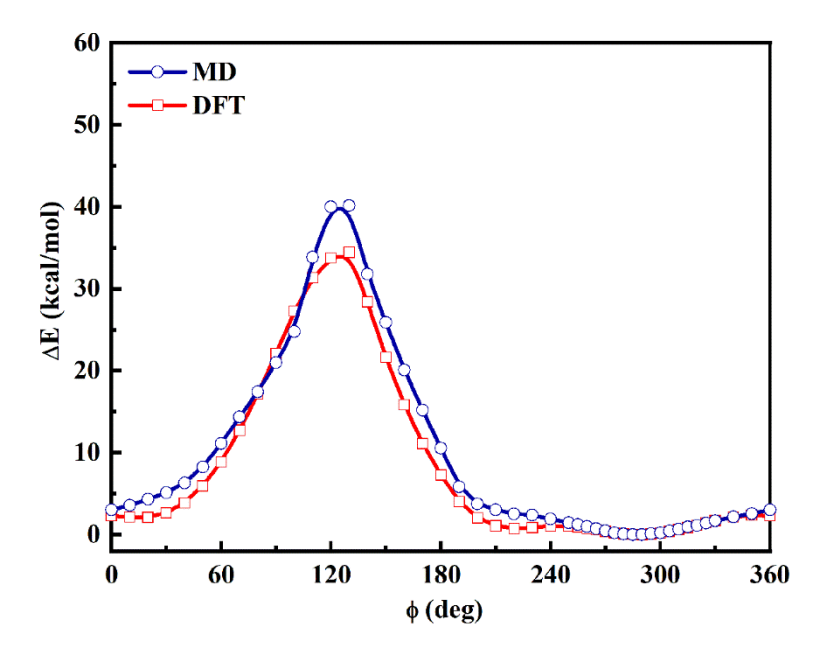


**Figure S5**. Complete torsion energy profiles for Au(s)-S(m)-C-H dihedral angle in the staple motif model obtained from MD and DFT calculations.

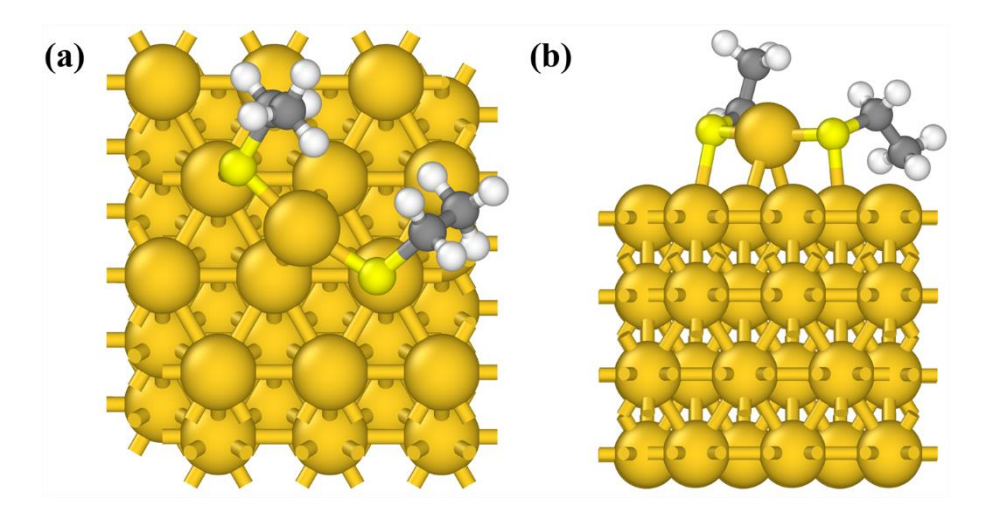


**Figure S6**. (a) top and (b) side views of the staple motif configuration where the dihedral angle of Au(s)-S(m)-C-C is 260°. Color code: Au, gold; S, yellow; C, gray; H, white.

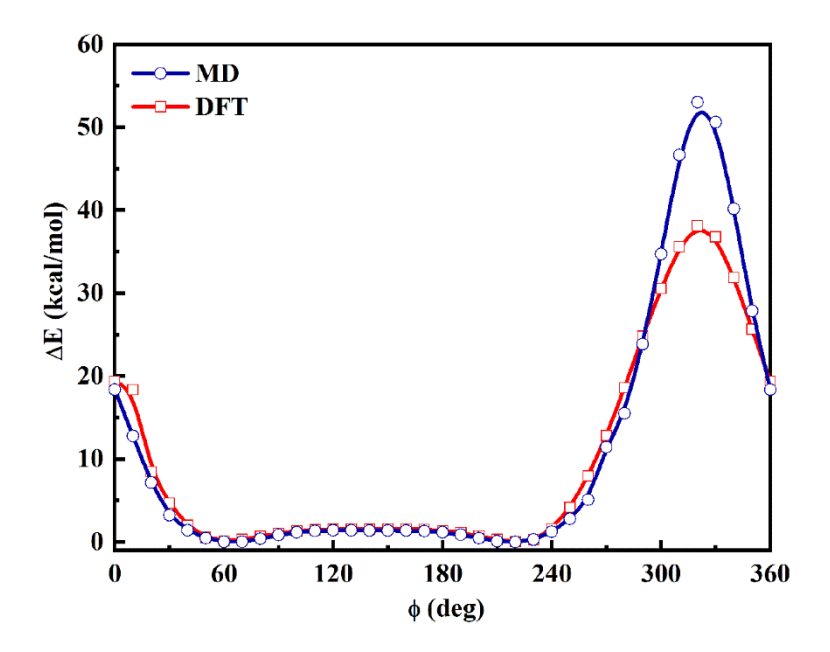


**Figure S7**. Complete torsion energy profiles for Au(s)-S(b)-C-C in dihedral angle the bridge model obtained from MD and DFT calculations.

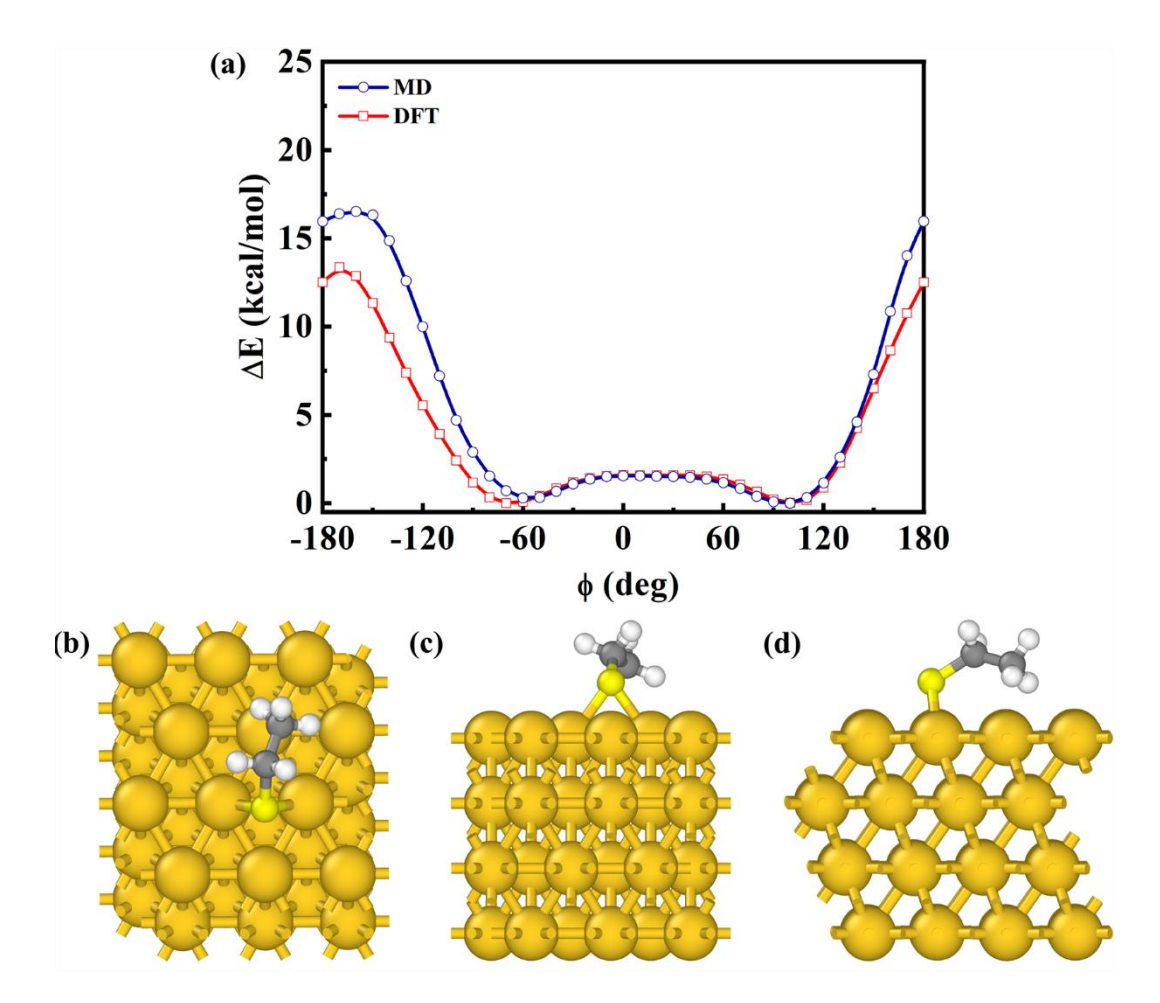


**Figure S8**. (a) Complete torsion energy profiles for Au(s)-S(b)-C-H dihedral angle in the bridge model obtained from MD and DFT calculations, (b) top and (c, d) side views of the bridge configuration where the dihedral angle of Au(s)-S(b)-C-H is -180° (180)°. Color code: Au, gold; S, yellow; C, gray; H, white.

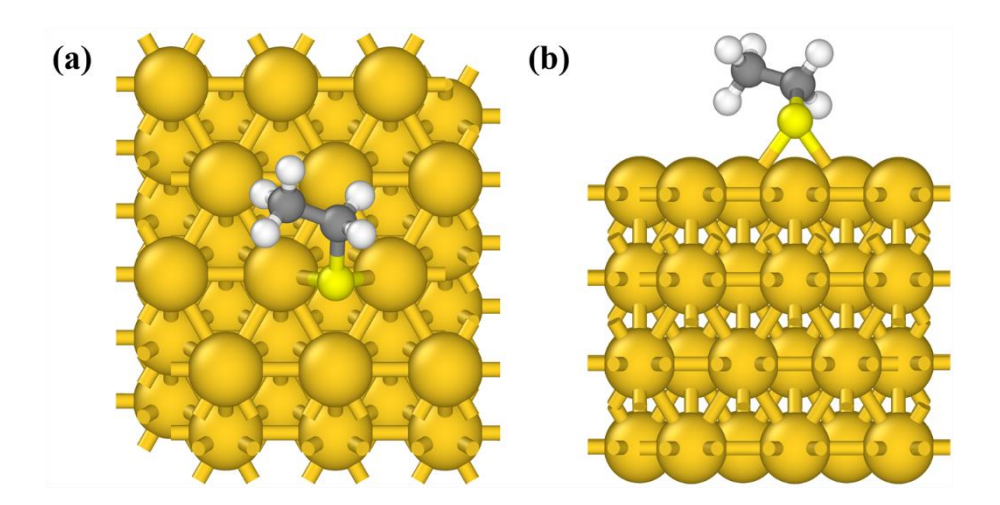


**Figure S9**. (a) top and (b) side views of the bridge configuration where the dihedral angle of Au(s)-S(b)-C-H is -70 (290)°. Color code: Au, gold; S, yellow; C, gray; H, white.

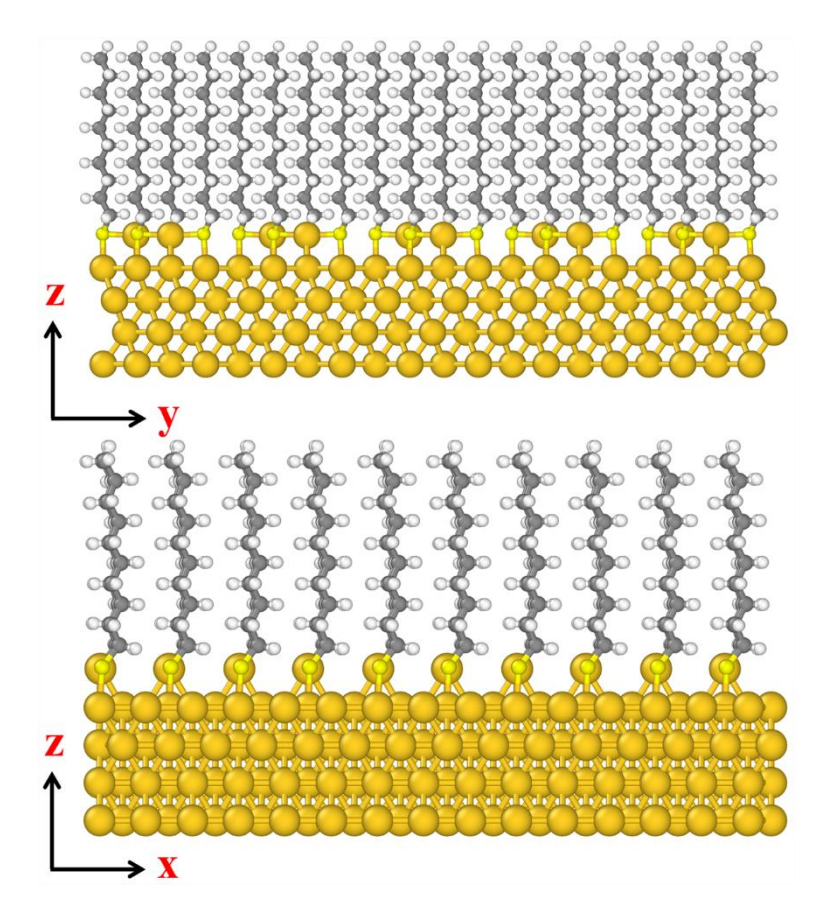


**Figure S10.** Side views of the initial configuration for model A with the unit  $(2\sqrt{3}\times3)$  unit cell being duplicated  $5\times5$  in x and y directions, respectively. Color code: Au, gold; S, yellow; C, gray; H, white.

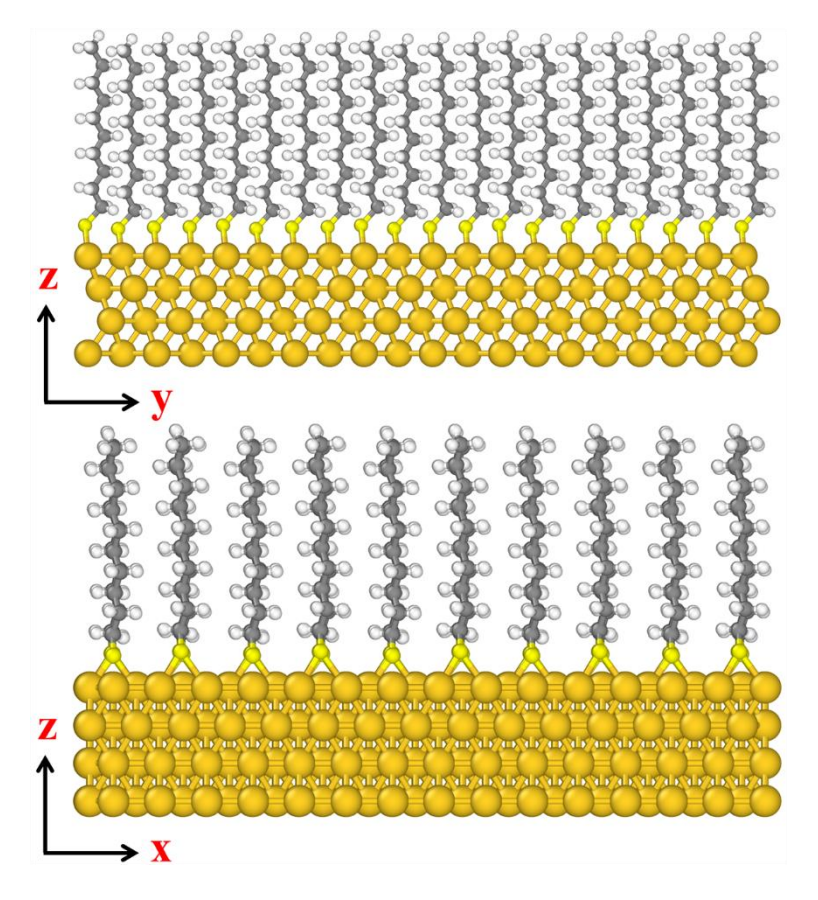


**Figure S11.** Side views of the initial configuration for model B with the unit  $(2\sqrt{3}\times3)$  unit cell being duplicated  $5\times5$  in x and y directions, respectively. Color code: Au, gold; S, yellow; C, gray; H, white.

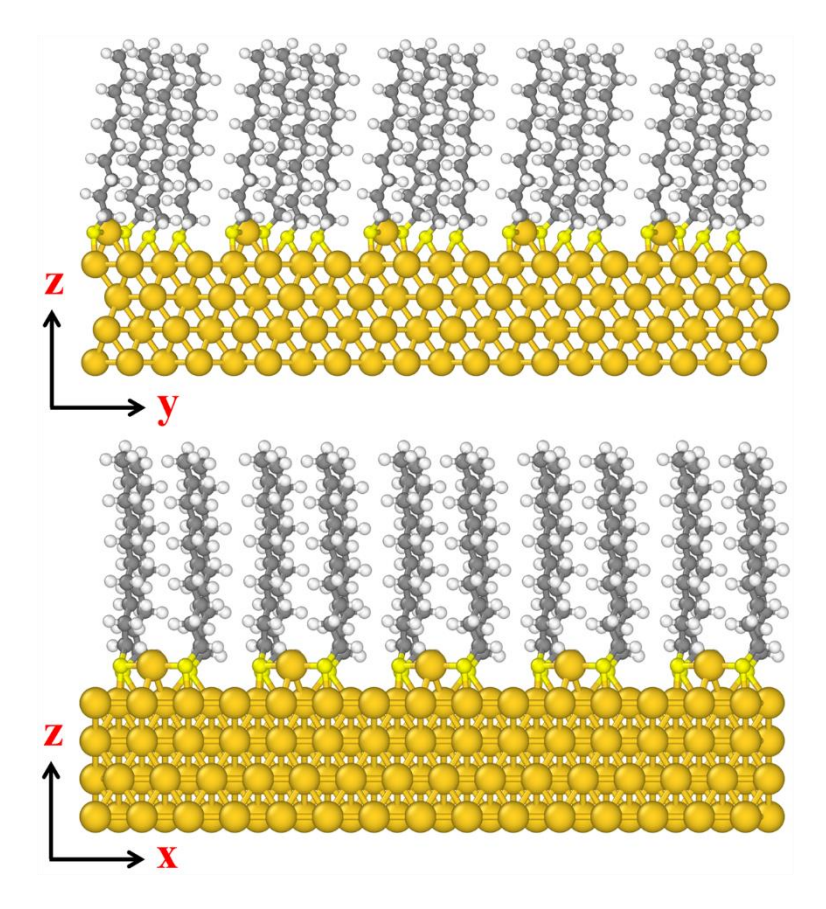


**Figure S12.** Side views of the initial configuration for model C with the unit  $(2\sqrt{3}\times3)$  unit cell being duplicated  $5\times5$  in x and y directions, respectively. Color code: Au, gold; S, yellow; C, gray; H, white.

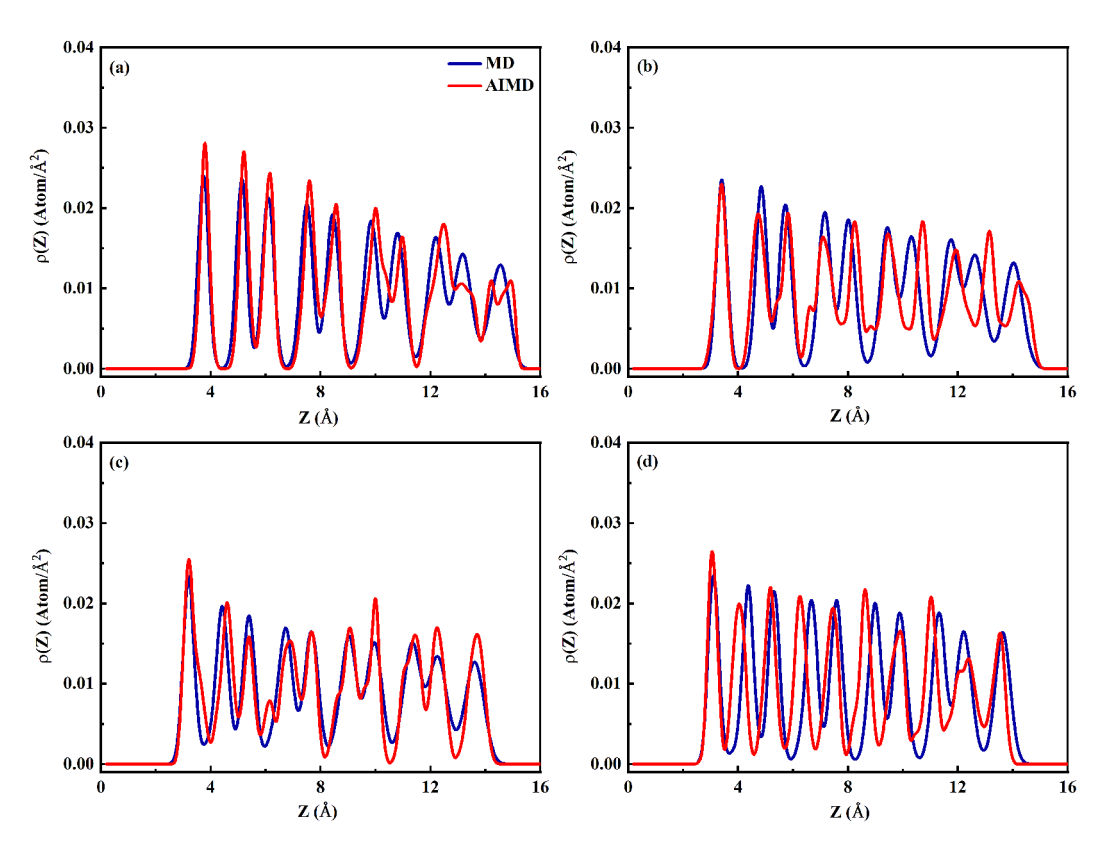


**Figure S13.** Density distributions of the C atoms in alkane chain along the z direction for (a) molecule 1, (b) molecule 2, (c) molecule 3, and (d) molecule 4 in model C at 200.0 K. The four molecules are denoted as M1, M2, M3, and M4 in Figure S14.

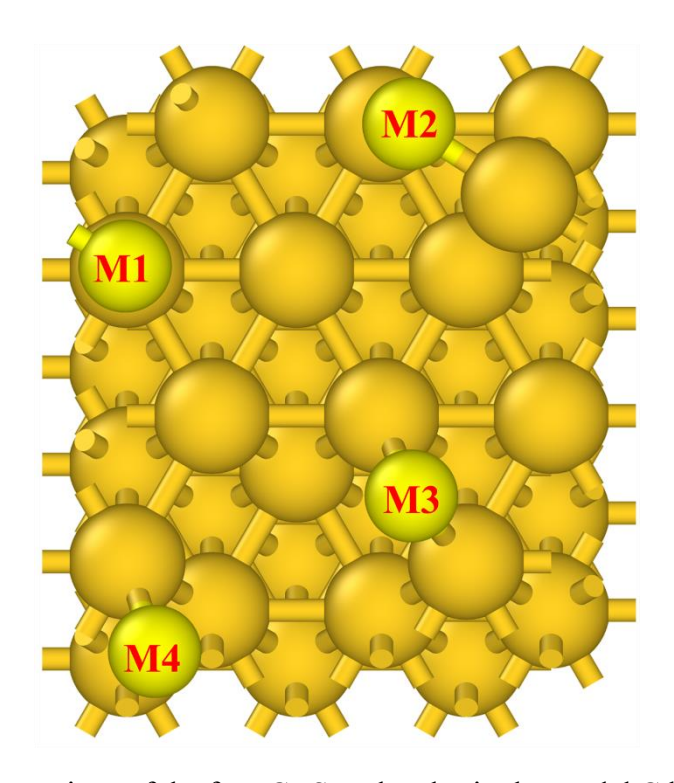


**Figure S14.** The notations of the four  $C_{10}S$  molecules in the model C listed in Figure 3.

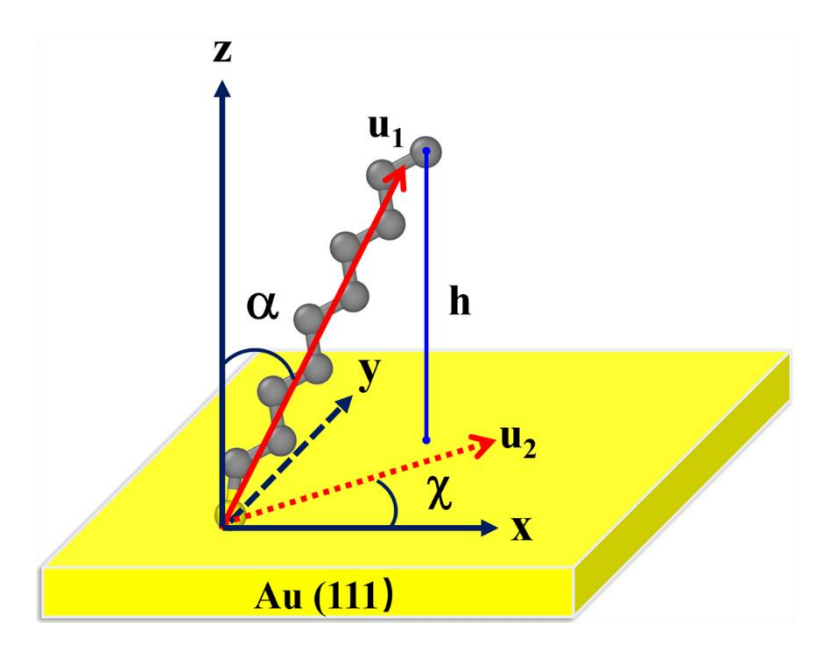


Figure S15. Schematic illustrations for the vectors and angles used in this study. Note:  $\mathbf{u}_1$  is the vector passing through the S atom and the centroid of each chain;  $\mathbf{u}_2$  is the projection of vector  $\mathbf{u}_1$  in x-y plane. Tilt angle  $\alpha$  is formed between the surface normal vector and vector  $\mathbf{u}_1$ , and the azimuthal angle  $\chi$  is defined as the angle between vector  $\mathbf{u}_2$  and the unit vector along the x-direction.

# Force Field Parameter Development for the Thiolate/Defective Au (111)

#### Interface

Guobing Zhou,<sup>a</sup> Chang Liu,<sup>b</sup> Lloyd A. Bumm,<sup>c</sup> Liangliang Huang<sup>\*a</sup>

(a) School of Chemical, Biological and Materials Engineering, University of Oklahoma,

Norman, Oklahoma 73019, United States

(b) State Key Laboratory of Materials-Oriented Chemical Engineering, Nanjing Tech University,

Nanjing 210009, China

(c) Homer L. Dodge Department of Physics and Astronomy, University of Oklahoma, Norman,

Oklahoma 73019, United States

## **Supporting Information 2**

This document shows the steps to develop the force constants for bond, angle, and torsional terms studied in the present study. Files mentioned in the text below are provided for your reference and all executables mentioned below are for Windows OS, and the Linux version can be found on the website (https://dasher.wustl.edu/tinker).

Part 1: Procedures to obtain the force constants for bonds and angles via matching the vibrational frequency.

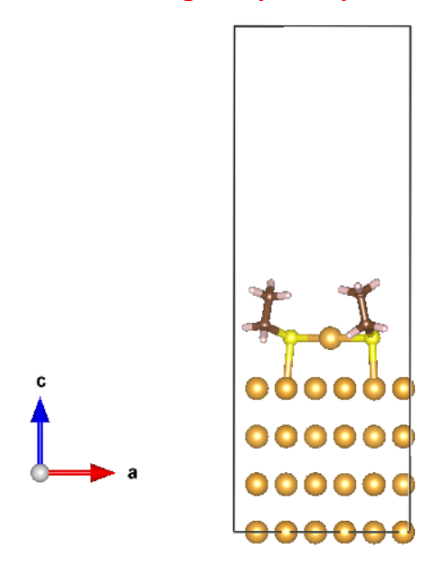
#### **Needed softwares:**

- (1) **Tinker-**Ver. 7.1 (https://dasher.wustl.edu/tinker/)
- (2) Force Field Explorer-Ver. 6.0 (https://dasher.wustl.edu/tinker/)

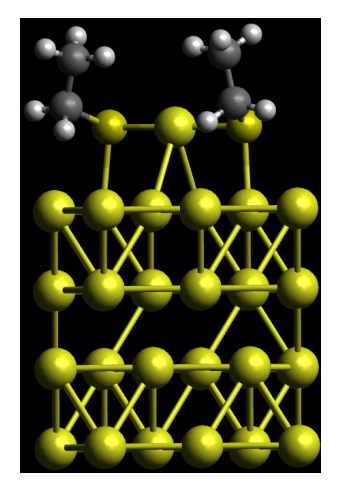
- (3) **VASP-**Ver. 5.4.1
- (4) **Jmol**-Ver. 14.29.26 (http://jmol.sourceforge.net/)
- (5) **VESTA-**Ver. 3.4.7 (http://jp-minerals.org/vesta/en/)
- (6) Avogadro-Ver. 1.2.0 (https://avogadro.cc/)

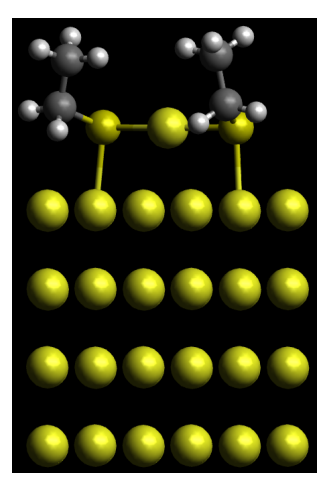
#### Steps:

- **1. Structural optimization** (see files in **1\_optimization** folder): this part of optimization is for the initial staple motif structure on the Au (111) surface.
- 2. Vibrational frequency calculation (see files in 2\_vibrational frequency calculation folder);
- 3. Convert CONTCAR to xyz (all files mentioned below are in 3\_contcar2xyz folder)
- (1) Open "CONTCAR" in 2\_vibrational frequency analysis folder with VESTA

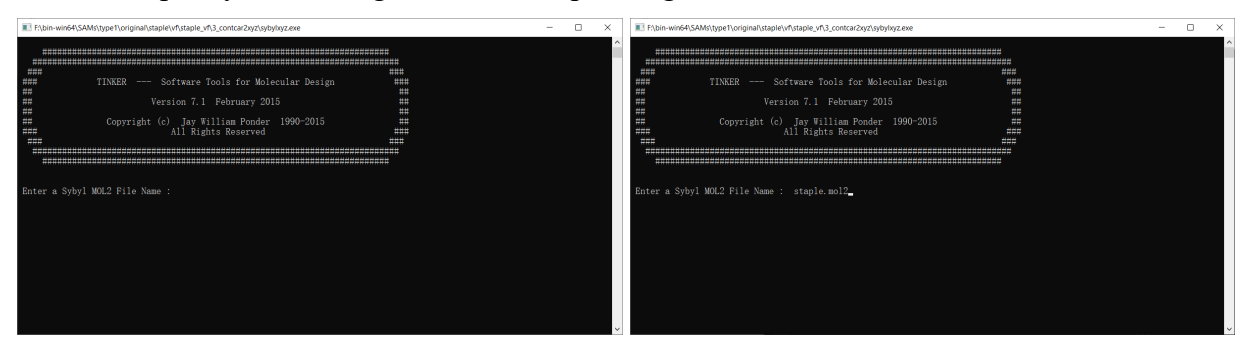


- (2) From the "File" menu, choose "Export Data", save the file in pdb format in 3\_contcar2xyz folder. By now, you shall have a file, named "staple.pdb".
- (3) Open staple.pdb file with Avogadro (see the left figure below) and then delete all the bonds between the Au atoms in the substrate (see the right figure below)





- (4) From the "File" menu, choose "Save As", save the file in the mol2 format. By now, you shall have a file, named "staple.mol2"
- (5) Convert the staple.mol2 file to .xyz file (Note: the xyz file of Tinker has a different format from the general xyz format).
- (I) Double click the sybylxyz.exe executable and then import the staple.mol2 file. A new file named "staple.xyz" will be generated after pressing the enter button.



(II) Prepare the .key file, which contains simulation settings and parameters. Visit the website (<a href="https://dasher.wustl.edu/tinker/">https://dasher.wustl.edu/tinker/</a>) for more details about the .key file. The descriptions of the .key file are listed below. To successfully run the following steps, you need to assign initial guess values for the force constants of the bonds, angles, and dihedrals (Note: 0.0 is not always a good choice since it may result in some errors).

	Atom Type		Comment		Atomic Weight	Bond Number
atom	1	Au	"bulk Au atom"	79	196.966	0
atom	2	Au	"bulk Au atom bonded with	S" 79	196.966	1
atom	3	Au	"Au adatom bonded with S"	79	196.966	2
atom	4	S	"S atom in C2S thiolate"	16	32.065	3
atom	5	C	"C atom in CH2"	6	12.027	4
atom	6	C	"C atom in CH3"	6	12.027	4
atom	7	H	"H atom in CH2 and CH3"	1	1.008	1

(III) After getting the .key file (see the staple.key file in 3\_contcar2xyz folder), open the staple.xyz file and add the atom type for each atom. To distinguish the edited xyz file and the original one, the original xyz file from step (I) was named as staple\_2.xyz.

	Origin	al staple.x	xyz (staple	_2.xyz for	now)	)			n	xyz	Atom Type	
65	****					1	65					
1	Au	1.127000	3.019000	0.002000	0	1 1	1	Au	1.127000	3.019000	0.002000	1
2	Au	1.127000	8.041000	0.002000	0		2	Au	1.127000	8.041000	0.002000	1
3	Au	2.577000	5.530000	0.002000	0		3	Au	2.577000	5.530000	0.002000	1
4	Au	2.577000	0.509000	0.002000	0		4	Au	2.577000	0.509000	0.002000	1
5	Au	4.026000	3.019000	0.002000	0		5	Au	4.026000	3.019000	0.002000	1
6	Au	4.026000	8.041000	0.002000	0		6	Au	4.026000	8.041000	0.002000	1
7	Au	5.476000	0.509000	0.002000	0		7	Au	5.476000	0.509000	0.002000	1
8	Au	5.476000	5.530000	0.002000	0		8	Au	5.476000	5.530000	0.002000	1
9	Au	6.925000	8.041000	0.002000	0		9	Au	6.925000	8.041000	0.002000	1
10	Au	6.925000	3.019000	0.002000	0		10	Au	6.925000	3.019000	0.002000	1
11	Au	8.375000	0.509000	0.002000	0		11	Au	8.375000	0.509000	0.002000	1
12	Au	8.375000	5.530000	0.002000	0		12	Au	8.375000	5.530000	0.002000	1
13	Au	1.127000	1.346000	2.369000	0		13	Au	1.127000	1.346000	2.369000	1
14	Au	1.127000	6.367000	2.369000	0		14	Au	1.127000	6.367000	2.369000	1
15	Au	2.577000	3.856000	2.369000	0		15	Au	2.577000	3.856000	2.369000	1
16	Au	2.577000	8.878000	2.369000	0		16	Au	2.577000	8.878000	2.369000	1
17	Au	4.026000	1.346000	2.369000	0		17	Au	4.026000	1.346000	2.369000	1
18	Au	4.026000	6.367000	2.369000	0		18	Au	4.026000	6.367000	2.369000	1
19	Au	5.476000	8.878000	2.369000	0		19	Au	5.476000	8.878000	2.369000	1
20	Au	5.476000	3.856000	2.369000	0		20	Au	5.476000	3.856000	2.369000	1
21	Au	6.925000	1.346000	2.369000	0		21	Au	6.925000	1.346000	2.369000	1
22	Au	6.925000	6.367000	2.369000	0		22	Au	6.925000	6.367000	2.369000	1
23	Au	8.375000	3.856000	2.369000	0		23	Au	8.375000	3.856000	2.369000	1
24	Au	8.375000	8.878000	2.369000	0		24	Au	8.375000	8.878000	2.369000	1

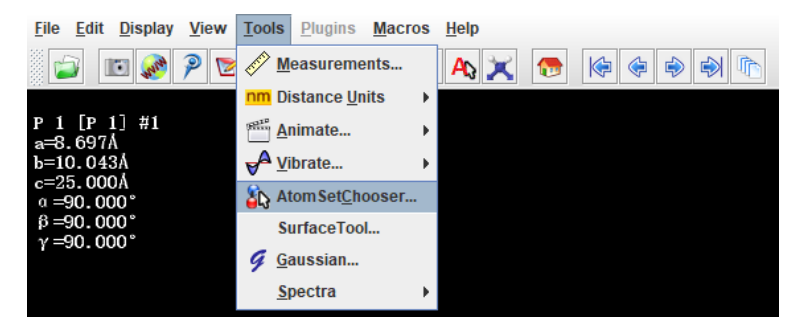
40	2	2.577000	5.530000	7.104000	0	51													
	Au					21				40	Au	2.577000	5.530000	7.104000	2	51			
41	Au	4.026000	3.019000	7.104000	0					41	Au	4.026000	3.019000	7.104000	1				
42	Au	4.026000	8.041000	7.104000	0					42	Au	4.026000	8.041000	7.104000	1				
43	Au	5.476000	0.509000	7.104000	0					43	Au	5.476000	0.509000	7.104000	1				
44	Au	5.476000	5.530000	7.104000	0					44	Au	5.476000	5.530000	7.104000	1				
45	Au	6.925000	8.041000	7.104000	0					45	Au	6.925000	8.041000	7.104000	1				
46	Au	6.925000	3.019000	7.104000	0	50				46	Au	6.925000	3.019000	7.104000	2	50			
47	Au	8.375000	0.509000	7.104000	0					47	Au	8.375000	0.509000	7.104000	1				
48	Au	8.375000	5.530000	7.104000	0					48	Au	8.375000	5.530000	7.104000	1				
49	Au	4.760000	4.300000	9.590000	0	50	51			49	Au	4.760000	4.300000	9.590000	3	50	51		
50	S	6.821000	3.235000	9.605000	0	46	49	52		50	S	6.821000	3.235000	9.605000	4	46	49	52	
51	S	2.806000	5.546000	9.614000	0	40	49	54		51	S	2.806000	5.546000	9.614000	4	40	49	54	
52	C	6.518000	1.553000	10.279000	0	50	53	56	57	52	C	6.518000	1.553000	10.279000	5	50	53	56	57
53	C	6.227000	1.590000	11.771000	0	52	58	59	60	53	C	6.227000	1.590000	11.771000	6	52	58	59	60
54	C	1.499000	4.404000	10.211000	0	51	55	61	62	54	C	1.499000	4.404000	10.211000	5	51	55	61	62
55	C	1.731000	3.923000	11.633000	0	54	63	64	65	55	C	1.731000	3.923000	11.633000	6	54	63	64	65
56	H	7.434000	0.989000	10.047000	0	52				56	H	7.434000	0.989000	10.047000	7	52			
57	H	5.697000	1.091000	9.710000	0	52				57	H	5.697000	1.091000	9.710000	7	52			
58	H	7.042000	2.071000	12.330000	0	53				58	H	7.042000	2.071000	12.330000	7	53			
59	H	6.109000	0.565000	12.153000	0	53				59	H	6.109000	0.565000	12.153000	7	53			
60	H	5.300000	2.144000	11.979000	0	53				60	H	5.300000	2.144000	11.979000	7	53			
61	H	1.435000	3.557000	9.507000	0	54				61	H	1.435000	3.557000	9.507000	7	54			
62	H	0.563000	4.973000	10.114000	0	54				62	H	0.563000	4.973000	10.114000	7	54			
63	H	2.649000	3.320000	11.698000	0	55				63	H	2.649000	3.320000	11.698000	7	55			
64	H	0.883000	3.296000	11.948000	0	55				64	H	0.883000	3.296000	11.948000	7	55			
65	H	1.820000	4.761000	12.318000	0	55				65	H	1.820000	4.761000	12.318000	7	55			

(IV) Before moving forward, for the staple.xyz file, we need to translate the center of mass to the origin. Steps: (a) copy the staple.xyz and staple.key files to translate the center of mass to the origin folder; (b) double click the xyzedit.exe executable; (c) input the staple.xyz file and press the Enter button; (d) input the number of the desired choice (here we choose NO. 12) and press the Enter button. This operation will generate a new file named as staple.xyz\_2. To distinguish these two files, the old stape.xyz was named as staple\_2.xyz and the new staple.xyz\_2 was named as staple.xyz. Then, copy staple.xyz and staple.key files to 4\_vibrational frequency fitting folder.

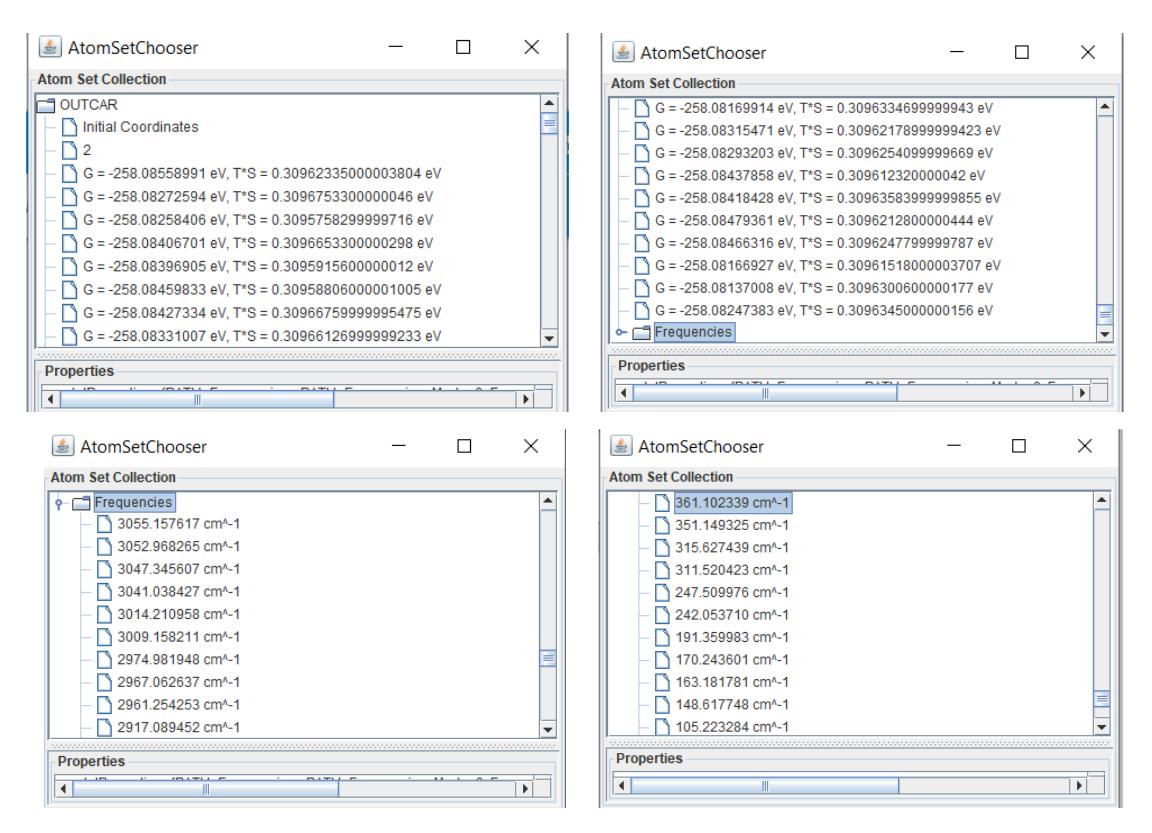


## 4. Vibrational frequency fitting

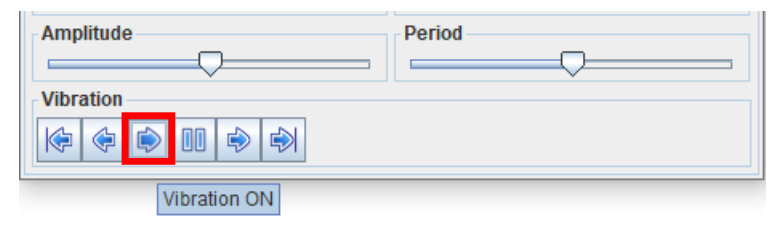
- (1) Copy the OUTCAR file from the 2\_vibrational frequency analysis folder. Open the OUTCAR file with Jmol to find the vibrational frequency for each vibrational mode.
- (2) Click the "Tools" and select "AtomSetChooser".



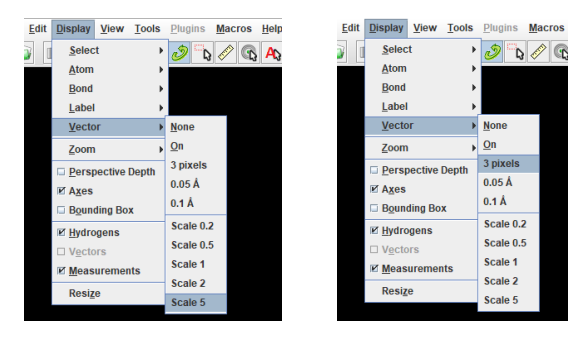
Scroll down to the end and then double click "**Frequencies**". Scroll down to find the vibrational spectra for the Au-S interface, which is in the range of 150-400 cm<sup>-1</sup>.



To visualize the vibration of each model, choose one frequency and then click the "**vibration on**" button (see below). (Here I choose the frequency 361.1 cm<sup>-1</sup> as the example to illustrate the fitting procedures below)

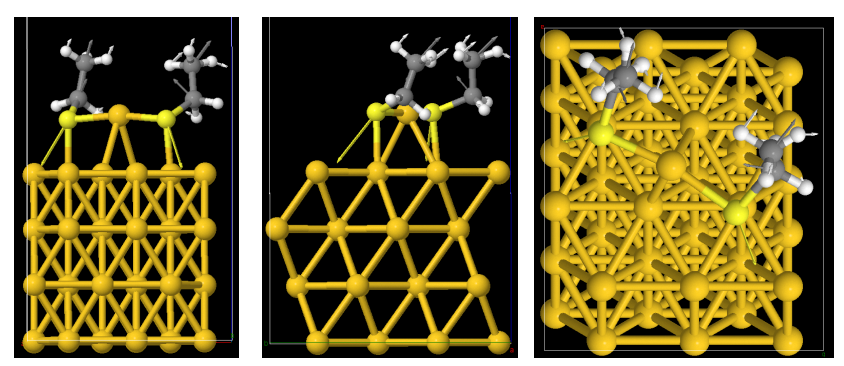


To make the vibration clearer, click "Display" button and select "Vector--> Scale 5", as well as "Vector--> 3 pixels":

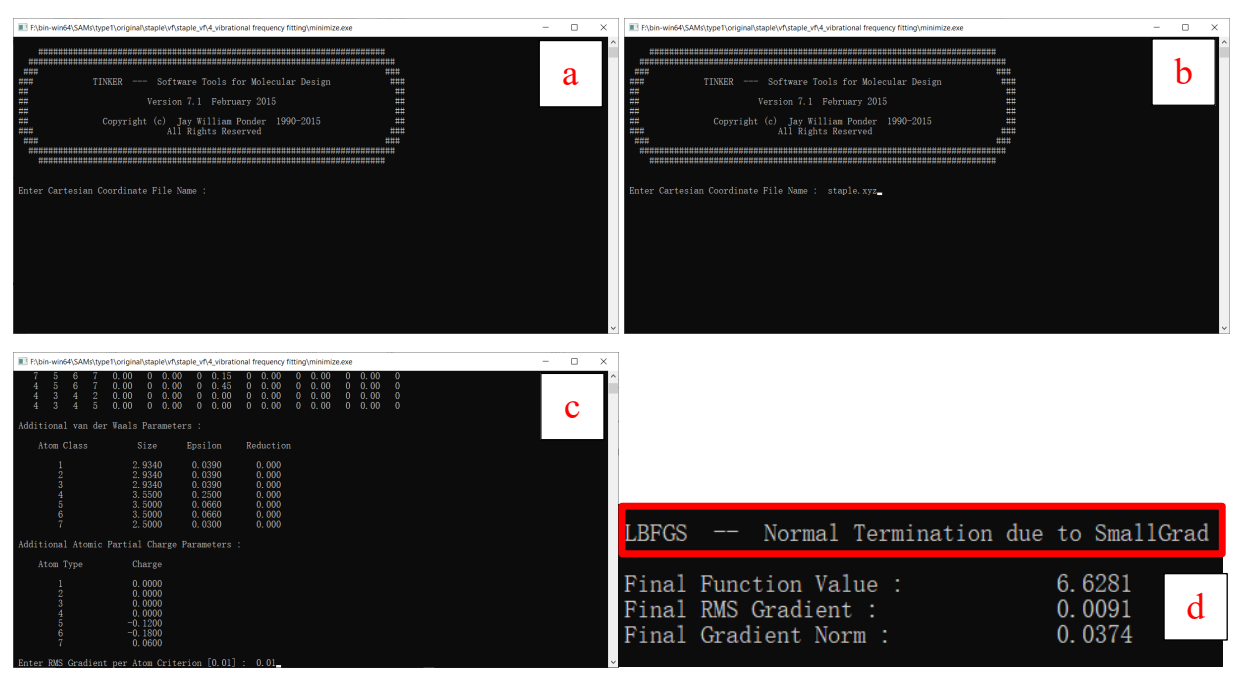


The vibrations from different views are listed below. Based on the vibrations, the frequency 361.1 cm<sup>-1</sup> corresponds to the angle Au(a)-S(m)-C bending mode. The value from DFT calculation

is used as the reference value for the MD fitting. Note: the identification of vibrational mode in this step is very important since it determines whether you have the correct reference state, including vibrational frequency and vibrational mode, for the later MD fitting.

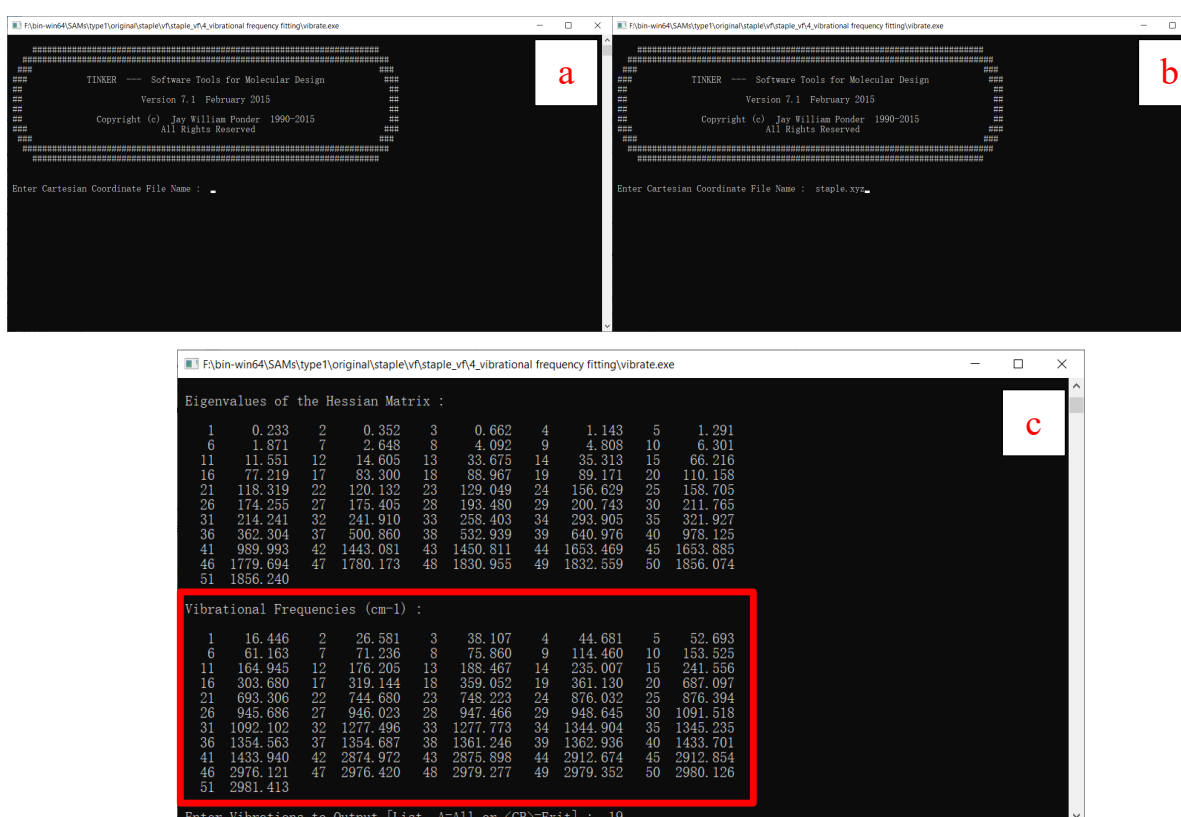


(3) We then need to optimize the structure with the minimize.exe executable: (a) double click the minimize.exe executable; (b) input the staple.xyz file and press the Enter button; (c) input the converged criterion (generally the default value is satisfactory) and the optimization will start after pressing press the Enter button; (d) the optimization would finish once it reaches the criteria. After the minimization, it would generate a new file named staple.xyz\_2 and we need to replace the staple.xyz by the new staple.xyz\_2. To maintain these two files, the old staple.xyz was named as staple\_old.xyz

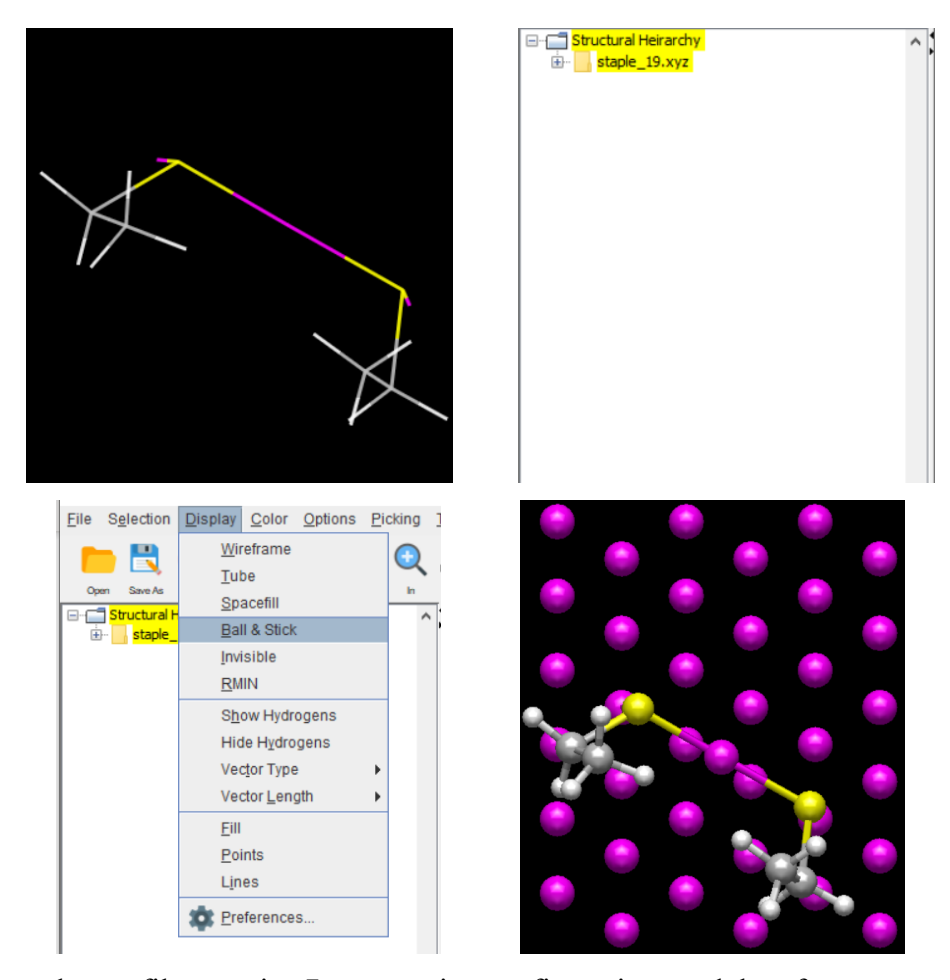


(4) Use the VIBRATE module to analyze the vibrational frequency:(a) double click the vibrate.exe executable; (b) input the staple.xyz file and press the Enter button. We can see the vibrational frequencies obtained from MD simulations. Basically, the number of vibrational frequencies from

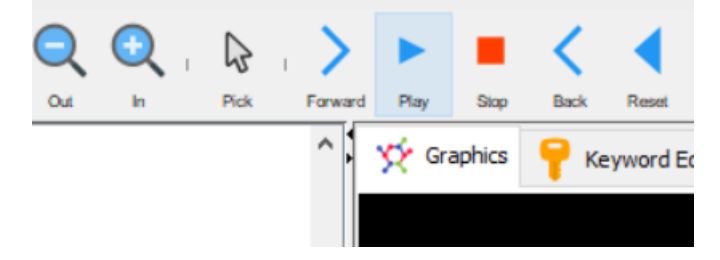
MD simulation should be the same as those from DFT calculation. In addition, each vibrational frequency corresponds to an integer number. (c) choose a vibrational frequency that is close to the DFT value (here we choose the 361.13 cm<sup>-1</sup> since the DFT value that we selected is 361.10 cm<sup>-1</sup>) and then enter the corresponding value. After pressing the Enter button, it would generate a new file named staple.019. We then change it to be staple\_19.xyz and copy staple.key to staple\_19.key. (Note: You may find slight difference for the vibrational frequencies in (c), probably due to the fact that each optimization may not generate the structures with exactly same coordinates)



(5) Afterwards, we can use the **Force Field Explorer** to open the staple\_19.xyz. Initially, you may observe only a part of the system (left figure of upper panel). To visualize the whole system, you need to do the following steps: (a) click and choose the staple\_19.xyz on the left; (b) click "**Display**" and choose "**Ball & Stick**". Then you can see the entire structure (right figure of lower panel).



Indeed, the staple.xyz file contains 7 consecutive configurations and therefore we can use the **Play** function in **Force Field Explorer** to observe the vibration of system.



The aim of doing this is to compare the vibrational modes of the selected frequencies from both MD and DFT. If the vibrational modes of the two frequencies are the same, we conclude that the correct vibrational frequency in MD for the Au(a)-S(m)-C bending mode has been identified.

In our provided examples, the finally obtained values are considered as the initial guess values for the force constants and therefore we can easily find out the correct vibrational frequency and modes in MD simulation. In the initial stage, however, it is always difficult to choose an appropriate initial guess value. In this case, one of the valuable tips is that the initial guess values

for the force constants of some new terms (bond, angle, and dihedrals) can be derived from the force field that contains similar local environment. With the initial guess values, we can do (3)-(5) of Step 4 to get the vibrational frequencies and modes for MD. Next, basically there would have two situations: (a) the obtained vibrational mode is the same to the one from DFT, but the vibrational frequency is different; (b) both the vibrational frequency and vibrational mode are distinct from the ones from DFT. For situation (a), once the vibrational mode is determined, you need to manually tune the force constant of corresponding term. Then we need to rerun (3)-(5) of Step 4 to get the vibrational frequency and compare it with the DFT reference value until they can agree with each other. For situation (b), we first need to run (4) of Step 4 to choose new vibrational frequencies and do the (5) of Step 4 to analyze the vibrational mode until we have the correct vibrational mode. After that, we only need to do the same operations as stated for situation (a) to get the force constant of targeted term. Use the aforementioned steps and operations for all interested bonds and angles, we can then obtain the desired force constants for them.

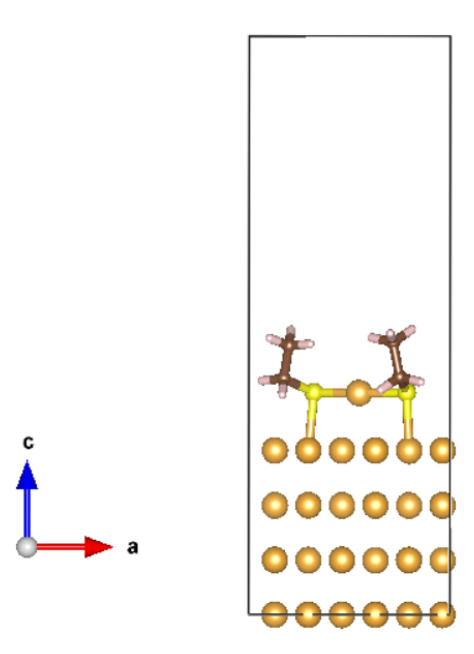
**Part 2:** Procedures to obtain the force constants for dihedrals via matching the torsional energy profiles. In this part, we use the Au(a)-S(m)-C-C torsion term as the example to show how to fit the torsional energy profiles.

#### **Needed softwares:**

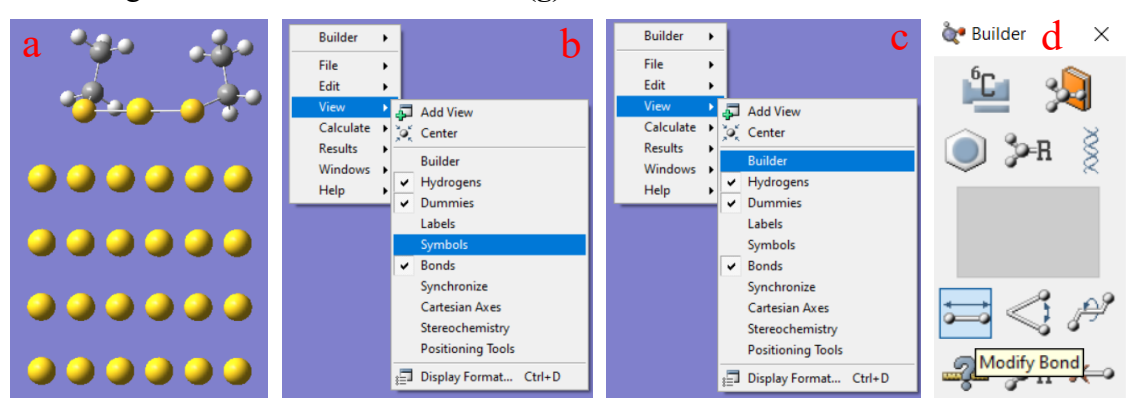
- (1) **Tinker-**Ver. 7.1 (https://dasher.wustl.edu/tinker/)
- (2) **VASP-Ver.** 5.4.1
- (3) VESTA-Ver. 3.4.7 (http://jp-minerals.org/vesta/en/)
- (4) GaussView-Ver. 4.1

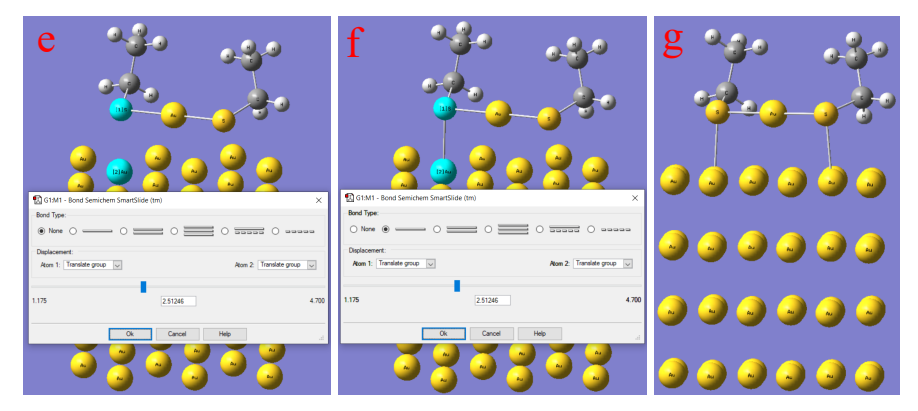
#### **Steps:**

- **1. Structural optimization** (see the files in **1\_optimization** folder): this part of optimization is for the initial staple motif structure on the Au (111) surface, which is the same as step 1 of Part 1.
- 2. Convert CONTCAR to pdb (see the files in 2\_contcar2pdb folder)
- (1) Copy CONTCAR from 1\_optimization folder to 2\_contcar2pdb folder. Open "CONTCAR" in 2 contcar2pdb folder with VESTA

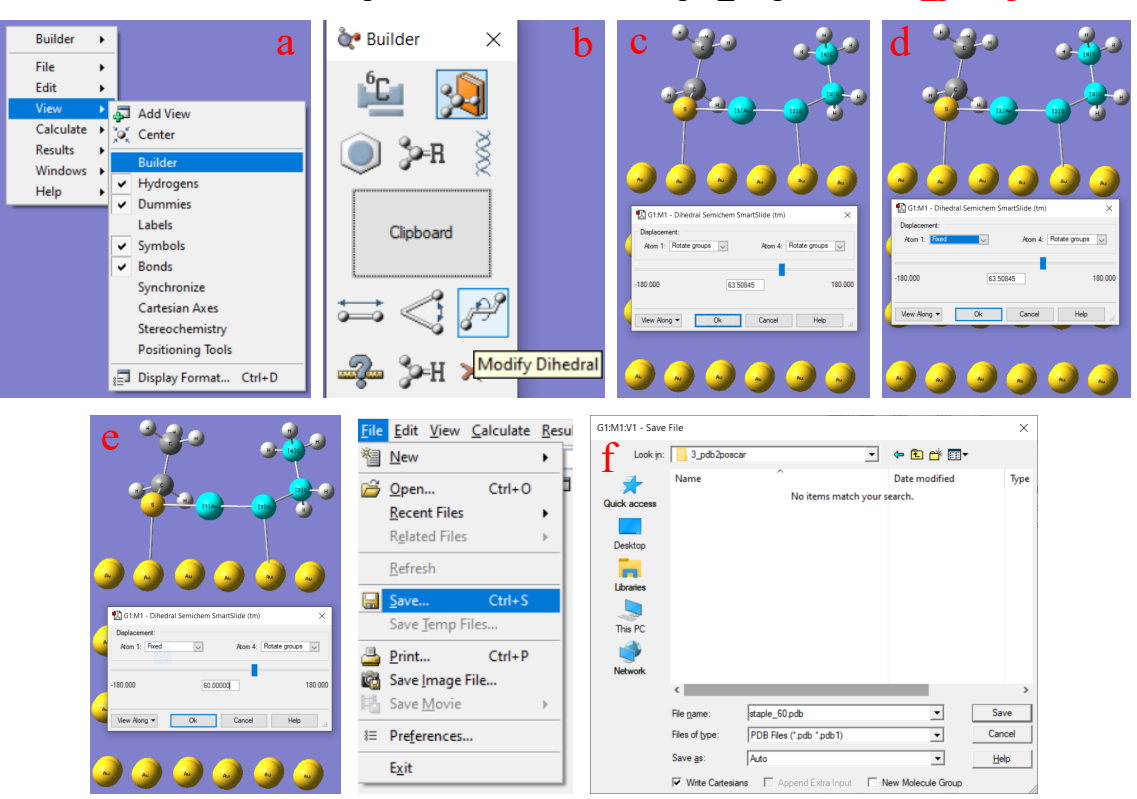


- (2) From the "File" menu, choose "Export Data", save the file in pdb format in 2\_contcar2pdb folder. By now, you shall have a file, named "staple.pdb".
- (3) For the Au(a)-S(m)-C-C torsion term, create 36 configurations with different dihedrals with an increase of 10°. A small interval like 5° can be used around the equilibrium dihedral value.
- (I) The following steps are used to create the bond connectivity between S atoms and Au atoms in the substrate in case there isn't any connectivity when you open the pdb file with GaussView: (a) Use GaussView to open the staple.pdb file; (b) Right click the mouse in main window and choose View-->Symbols to show the Symbols; (c) Right click the mouse in main window and choose View-->Builder; (d) choose the Modify Bond button; (e) select both S and Au atoms; (f) choose the second single bond and click OK button; (g) the bonds are created for S and Au atoms.

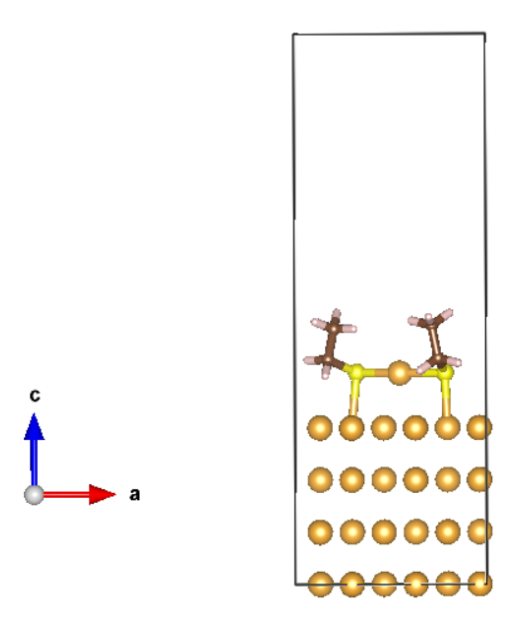




(II) The following steps are used to tune the dihedral for Au(a)-S(m)-C-C torsional term based on the configuration of (I): (a) Right click the mouse in main window and choose View-->Builder; (b) choose the Modify Dihedral button; (c) select Au adatom, S, C, and C atoms in sequence; (d) for atom1, change the Rotate groups to Fixed; (e) change the dihedral to be 60.0° and click OK. Here, we use the 60° value as an example and the procedures are the same for the other dihedrals. One thing should be noted is that the dihedral in GaussView is from -180° to 180° and therefore the dihedral in the range of -180° to 0° corresponds to 180° to 360°. (f) From the "File" menu, choose "Save...", save the file in pdb format, named as staple 60.pdb in the 3 pdb2poscar folder.



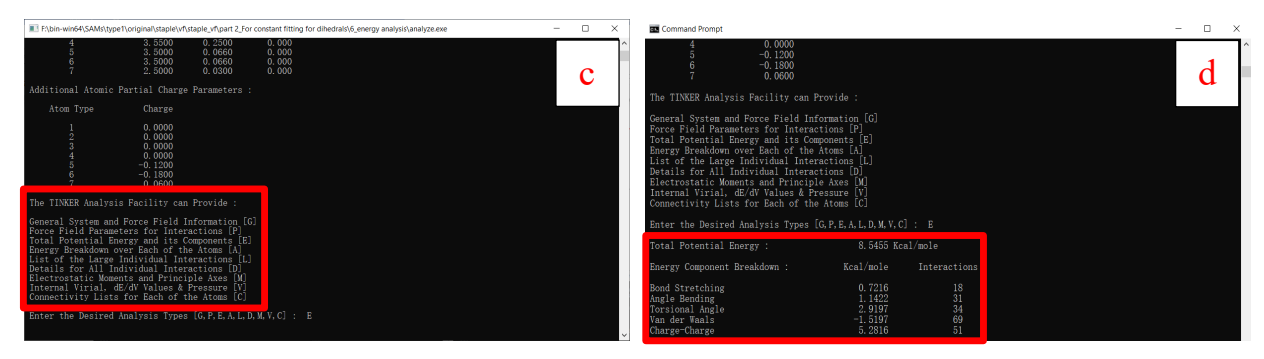
(III) Use the pdb2pos.f90 code to convert the staple\_60.pdb file to POSCAR (the files are in the 3 pdb2poscar folder). Open the POSCAR with VESTA to check the structure.



(IV) Structural optimization with VASP (see files in 4\_optimization for dihedral angle folder): this part of optimization is for the Au(s)-S(m)-C-C torsional term with specific dihedral. (a) copy the POSCAR from 3\_pdb2poscar folder to 4\_optimization for dihedral angle folder; (b) prepare additional three files, namely, INCAR, POTCAR, and KPOINT. After finishing the optimization, it would generate the CONTCAR file (see the files in 4\_optimization for dihedral angle folder) (V) Convert the CONTCAR file to .xyz file. In fact, we can use the steps in Part 1 to get the .xyz file from CONTCAR file. However, during the fitting process for the torsional terms, there are hundreds of CONTCAR to be converted into .xyz file. Therefore, a Fortran code cont2xyz.f90 has been prepared to simplify the conversion steps (see the files in 5 contcar2xyz folder).

(VI) Copy the final staple.key file from Part 1 and staple\_60.xyz from 5\_contcar2xyz folder to the 6\_ energy analysis folder and change the staple.key to be staple\_60.key. The following steps are carried out to calculate the total energy for MD: (a) double click the analyze.exe executable; (b) input the staple\_60.xyz and press the Enter button; (c) choose the third one and input the letter E; (d) we can get the MD total energy for the Au(a)-S(m)-C-C term with a dihedral of 60°.





**(VII)** Use the same method, we can get the MD total energy for the Au(a)-S(m)-C-C term with other dihedrals. Finally, we can obtain the MD total energy in the range of -180° to 180°. For both DFT and MD energies, find out the configuration with the lowest energy, which is then used as the reference value to calculate the energy difference as we display in the manuscript.

(VIII) Plot and compare the energy profiles from both DFT and MD. If there is a good agreement between them, the force constant would be the one that we want for the Au(a)-S(m)-C-C term. If not, we need to tune the force constant in the .key file and rerun the energy analysis as we described in VI) and VII) until we can get a good match between the DFT and MD results.

### Part 3: The computational resources

In part 1 of the Supporting Information 2, the CPU time for the DFT-based vibrational frequency calculation is about 4.6 and 1.6 hours for staple motif and bridge models, respectively, by using 48 cores. For the vibrational frequency fitting from MD, the time depends on the initial guess values of the force constant and it may vary from several days to one week. In part 2 of the Supporting Information 2, the computational resources mainly focus on the DFT optimization for the structures with different dihedrals and the torsional energy profiles fitting from MD. In regard to the optimization of each dihedral, the CPU time for the staple motif model varies from 0.2 (the most stable structure) to 12.5 hours (the least stable structure) by using 48 cores, and the optimization jobs are more than 150. In the case of bridge model, the corresponding CPU time varies from 0.5 (the most stable structure) to 3.7 hours (the least stable structure) with the same number of cores, and the optimization jobs are more than 70. For the force field validation simulations, the CPU time is about 40 hours for AIMD simulations to run 10 ps with 48 cores, while the corresponding time is about 100 hours for MD simulations to run 10 ns with 24 cores. All the calculations mentioned above were performed by using the high-performance supercomputers at University of Oklahoma and Nanjing Tech University.